Live imaging of heart tube development in mouse reveals alternating phases of cardiac differentiation and morphogenesis

Kenzo Ivanovitch[1], **Susana Temiño**[1], **Miguel Torres**[1*]

***For correspondence:**
mtorres@cnic.es (MT)

[1]Developmental Biology Program, Centro Nacional de Investigaciones Cardiovasculares Carlos III (CNIC), Madrid

Abstract During vertebrate heart development two progenitor populations, first and second heart fields (FHF, SHF), sequentially contribute to longitudinal subdivisions of the heart tube (HT), with the FHF contributing the left ventricle and most of the atria, and the SHF the rest of the heart. Here we study the dynamics of cardiac differentiation by tracking individual cells in live analysis of mouse embryos. We report unexpected temporal regulation of cardiac differentiation and its coordination with heart tube morphogenesis. During an initial phase, FHF precursors differentiate rapidly to form a cardiac crescent, while limited morphogenesis takes place. In a second phase, no differentiation occurs while extensive morphogenesis results in HT formation. In a third phase, cardiac precursor differentiation resumes and contributes to SHF-derived regions and the dorsal closure of the HT. These results reveal tissue-level coordination between morphogenesis and differentiation during HT formation and provide a new framework to understand heart development

Introduction

The heart is the first organ to form and function during embryonic development. At embryonic stage (E) 7.5, cardiac precursors in the splanchnic mesoderm (mesoderm apposed to the endoderm) differentiate into cardiomyocytes by assembling the contractile sarcomere machinery (Tyser et al., 2016) and form a bilateral structure known as the cardiac crescent (cc) in the mouse. Concomitant with foregut invagination, the cc swings inwards to become placed underneath the developing head folds. By a complex morphogenetic process, the cc subsequently transforms into an early heart tube (HT) initially opened dorsally, which by E8.25 has transformed into a closed and beating linear HT also known as the primitive HT (Evans et al., 2010; Kelly et al., 2014).

The cc and early HT mainly give rise to the left ventricle (Zaffran et al., 2004). The right ventricle (RV), the outflow track and most of the atria derive instead from cardiac progenitors located initially dorso-medially to the cc in the splanchnic mesoderm, that are progressively recruited at the poles of the HT at subsequent developmental stages (Cai et al., 2003; Kelly et al., 2001; Mjaatvedt et al., 2001; Waldo et al., 2005). These findings led to the concept that cardiac mesodermal progenitors contain two populations of cells: the first heart field (FHF) precursors, recruited early in development to form the early HT, and the second heart field (SHF), recruited later and elongating the HT (Buckingham et al., 2005). While clonal analysis (Devine et al., 2014; Lescroart et al., 2014; Meilhac et al., 2004a) supports the idea that FHF and SHF precursors are two independent developmental fields with

dedicated molecular pathways, the existence of a common precursor was also reported in the early mouse embryo (Meilhac et al., 2004a). Other views suggest that the heart forms by a continuous differentiation process from a single population of cardiac precursors and only timing of recruitment distinguish cells of the FHF and SHF (Abu-Issa et al., 2004; Moorman et al., 2007). In support of the latter, typical markers of the SHF, like Islet1 (Cai et al., 2003) are also expressed transiently in FHF precursors and must therefore be considered as pan-differentiation markers instead (Cai et al., 2003; Prall et al., 2007; Yuan and Schoenwolf, 2000). Whether the recruitment of cardiomyocytes from progenitors is a continuous process however has not been directly studied. This is partly because the spatial arrangement of progenitors and differentiated cardiomyocytes has so far been analysed on fixed embryos (Cai et al., 2003; Spater et al., 2013) and the expression dynamics of genes reporting differentiation together with cell movements during HT morphogenesis have not been captured so far (Abu-Issa, 2014).

Here, we report the live-imaging and 4D cell tracking of HT formation in whole mouse embryo. Using this method, in conjunction with an Nkx2.5eGFP reporter line, characterised by a high level of GFP in differentiated cardiomyocytes as compared to undifferentiated progenitors, we studied the dynamics of cardiac field differentiation. During an initial phase, FHF cardiac precursors differentiate rapidly to form a cardiac crescent, while limited morphogenesis takes place. During a second phase, no differentiation events are detected, while extensive morphogenesis results in HT formation. Finally, using an Isl1-Cre lineage tracing assay combined with live-imaging, we show that during a third phase, cardiac precursor differentiation resumes and contributes not only to the known SHF-derived regions but also to the dorsal aspect of the HT. These results show essential properties of FHF and SHF contribution to heart development and reveal tissue-level coordination between alternating phases of morphogenesis and differentiation during HT formation.

Results

3D static analysis of mouse HT formation

To assess how the initial cardiogenic region transforms into a HT and differentiates, we first analysed whole mouse embryos immunostained against cTnnT at successive embryonic stages. Figure 1-figure supplement-1 schematises the criteria for embryo staging (Downs and Davies, 1993; Kirstie A. Lawson, 2016). Cardiac troponin T (cTnnT) is one of the first evident sarcomeric proteins to appear in the cardiac crescent (Tyser et al., 2016). At early head fold stage (EHF, E7.5), the cardiogenic region is visualised in Nkx2.5cre+/- R26tdtomato+/- embryos, where both cardiac precursors and cardiomyocytes express Cre (Stanley et al., 2002). The tdtomato+ region in these embryos forms a flat horse shoe-shaped mesodermal layer at the rostral border of the embryo (Figure 1A,A', Video 1). At this stage, cTnnT protein is not yet detected (Figure 1B), although in some embryos weak cTnnT localisation in subsets of cells can be occasionally visualised (Figure 1-figure supplement 2A,A'). At a subsequent embryonic stage (E7.7), cTnnT signal reveals the cc, which is folding inwards. During folding, the cTnnT signal increases and cTnnT+ cardiomyocytes switch from a columnar epithelial shape to a rounded shape (Linask et al., 1997) (Figure 1C,D and Figure 1-figure supplement 2B,B') and separate from the endoderm, while maintaining a basal lamina at the endocardial side (inset in Figure 1D and Fig2. D). Morphogenetic changes starting at E8 subsequently lead to the initial formation of a hemitube whose major axis is transversal to the embryo A-P axis. We will refer to this stage as transversal HT (Figure 1E). Later, the tube adopts a more spherical shape very similar to the linear HT but still open dorsally. We will refer to this stage as open HT (Figure 1F). The HT eventually closes dorsally (Figure 1G, red arrows in Figure 1G") and a prominent outflow (OFT, the prospective RV) (Zaffran et al., 2004) becomes visible (yellow arrows in Figure 1G", Figure 1H, see also Video 2), completing linear HT formation at E8.25.

To assess the overall growth of the forming HT, we measured cTnnT+ tissue volume in segmented z-stacks, at the stages described above (Figure 1I and Figure 1-source data 1). During the first phase of cardiomyocyte differentiation, the cTnnT signal expands resulting in a cardiac crescent rapidly

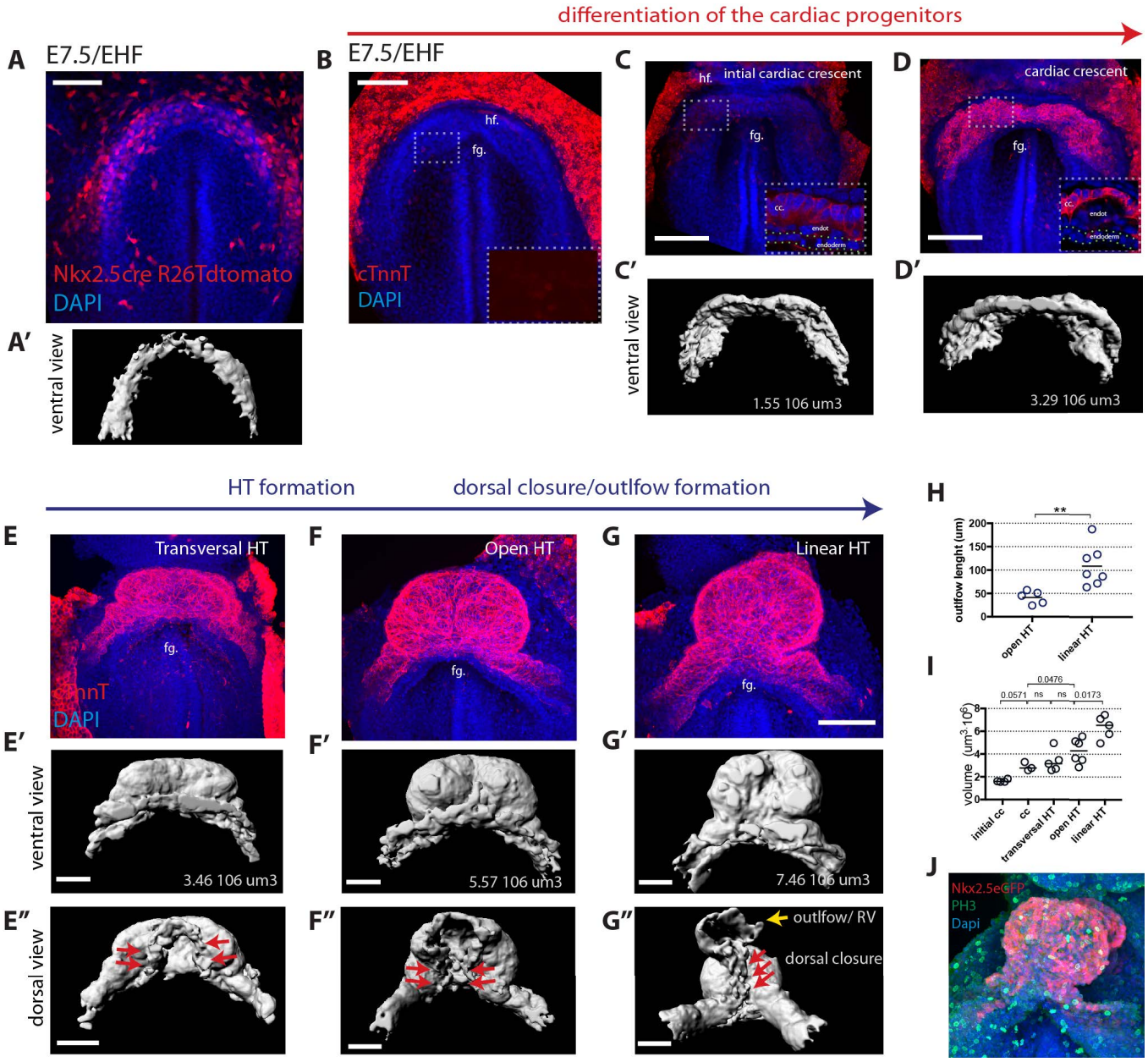

Figure 1. Overview of HT morphogenesis and growth. (A) Nkx2.5cre/+; R26tdtomato embryo at EHF stage. (A') 3D reconstruction. Signal from tdtomato+ endothelial cells identified by shape was manually masked. See also Video 1. (B-G) Immunostaining for cTnnT (red) and Dapi (blue) showing six consecutive stages during cardiac differentiation (B-D) and HT morphogenesis (E-G). (BB) At EHF cTnnt is initially not detectable. (C-D) During early somitogenesis, cTnnT signal in the cc becomes detectable. Insets in (B-D): magnification in single optical sections showing cTnnT localization and cell shape. (C'-G' and E"-G") Corresponding 3D renderings from cTnnT signal reconstruction. Red arrows in (E'-G') highlight the dorsal closure of the HT. Yellow arrow in G" highlights the outflow (prospective RV). See also Video 2. (H) Quantification of the outflow track/RV length in the HT (41.4 ±14.0 µm, n=5) and after (109 ±43.44 µm, n=7) dorsal closure, mean ± SD, p=0.0025. (I) Quantification of the volume at the different stages of HT development. (Initial cc: 1.63.106 µm3 ± 0.13, n=4, cc: 2.89.106 ± 0.37 µm3, n=3, transversal HT: 3.367.106 µm3 ± 0.95, n=5, open HT: 4.29.106 µm3 ± 1.08, n=6, linear HT: 6.37.106 µm3 ± 1.01, n=5, mean ± SD). P-values are indicated on the graph. (J) Immunostaining of an Nkx2.5eGFP embryo against PH3 (red) and Dapi (blue) at HT stage, showing proliferative cells in the ventricle. fg: foregut, endo: endoderm, endoc: endocardium. Scale bars: 150 µm.

Figure 1–Figure supplement 1. Criteria for staging Embryos.

Figure 1–Figure supplement 2. Faint cTnnT signal starts to be detected at EHF stage in apico-basally polarised cc cells.

Figure 1–source data 1.

doubling in volume (Figure 1C',D',I). During the subsequent phase of morphogenesis, from cc to open HT stage, growth is less pronounced despite extensive morphological changes (Figure 1E',F',I). Volume of the HT appears to increase again upon OFT addition and dorsal HT closure (Figure 1G',I). HT growth likely reflects an increase in cell number occurring during the formation of the heart tube. The cardiomyocytes are proliferative at this stage(de Boer et al., 2012), and we can indeed observe mitotic figures in the HT (Figure 1J). From this analysis, it is however unclear how much of the growth observed is due to cardiomyocyte proliferation versus addition of new cardiomyocytes from cardiac progenitor cells located in the splanchnic mesoderm.

3D analysis of cardiac progenitor differentiation

To visualise the boundary where cardiac progenitors abut differentiating cardiomyocytes during HT morphogenesis, we immunostained Nkx2.5cre+/- R26tdtomato+/- embryos with the differentiation marker cTnnT (Figure 2A). We acquired whole-mount images at transversal HT stage and rendered the Nkx2.5 lineage and the cTnnT+ tissues in 3D allowing visualising the boundary between cardiac progenitors and differentiated cardiomyocytes at tissue level (Figure 2A,B,B' and Video 3). While cardiomyocytes are separated from the endoderm by the endocardium, undifferentiated cardiac precursors lie medio-dorsally and remain in contact with the endoderm (Figure 1A',A''). The cell shape of progenitors and cardiomyocytes is also distinct. Membrane-GFP marking of single cells shows that cTnnT- progenitors have epithelial-like columnar cell shape while the differentiated cTnnT+ cardiomyocytes are rounder and lost the columnar epithelial organisation (Figure 2C-E and Figure 2-source data 1). This is reminiscent of the cell shape transition observed in the distal outflow track at later stages of heart development, when SHF progenitor-to-cardiomyocyte differentiation takes place (Francou et al., 2014; Ramsbottom et al., 2014; Sinha et al., 2012). Interestingly, some cells within the boundary zone exhibit weak cTnnT localisation and yet show columnar shapes typical of mesodermal cardiac precursors (Figure 2F-F'''' and red arrows in Figure 2F''',F''''). Since these cells do not show rounded shapes, as differentiated cardiomyocytes do, they may represent a transient state between progenitors and differentiated cardiomyocytes, however, the nature of such state cannot be addressed by static analysis. Differentiation of cardiac progenitors is thus accompanied by changes in cell shape and detachment from the endoderm.

We next assessed the expression pattern of the Nkx2.5eGFP enhancer reporter line, in which GFP is expressed in cardiomyocytes (Lien et al., 1999) (Wu et al., 2006). We immunostained Nkx2.5eGFP embryos against cTnnT, (Figure 3A,B and Figure 3- figure supplement 1A,B) and compared the relative intensities between cTnnT and GFP within single cells segmented manually (Figure 3C,D Figure 3- figure supplement 2A and Figure 3-source data 1). We found variable GPF level within both populations of cTnnT+ and cTnnT- cells. However, the top 50% cells with the highest GFP level were systematically positive for cTnnT+ (, Figure 3-source data 1) while cells with lower level of GFP were instead either positive or negative for cTnnT, and GFP level varied linearly with cTnnT level (Figure 2D). This confirms a previous report showing that Nkx2.5GFP+ differentiated cardiomyocytes were characterised by 5-fold higher mean levels of Nkx2.5GFP compared to SHF subpopulations in an Nkx2.5GFP knock-in mouse model (Prall et al., 2007) (Biben et al., 2000). However, cells expressing low level of GFP could also be cTnnT-positive, consistent with studies showing that SHF progenitors can contribute to the myocardium in the absence of Nkx2.5 expression (Christoffels et al., 2006). Genetic tracing experiments using the Nkx2.5-Cre Rosa26R-tdtomato line instead shows strong tdtomato level in both the FHF and SHF (Figure 3- figure supplement 3A). We next imaged the boundary between cardiomyocytes and cardiac precursors in transversal HT stage embryos. We measured mean fluorescent intensity in manually segmented cells at the boundary zone and found that an increase in GFP level correlates with the onset of detectable cTnnT localisation (Figure 3B',E, Figure 3- figure supplement 2B,C and Figure 3-source data 1). Altogether, these results indicate that the Nkx2.5-eGFP reporter is suitable for tracking cardiomyocytes in live-imaging and reliably identifies the top 50% GFP-expressing cells as cTnnT-positive.

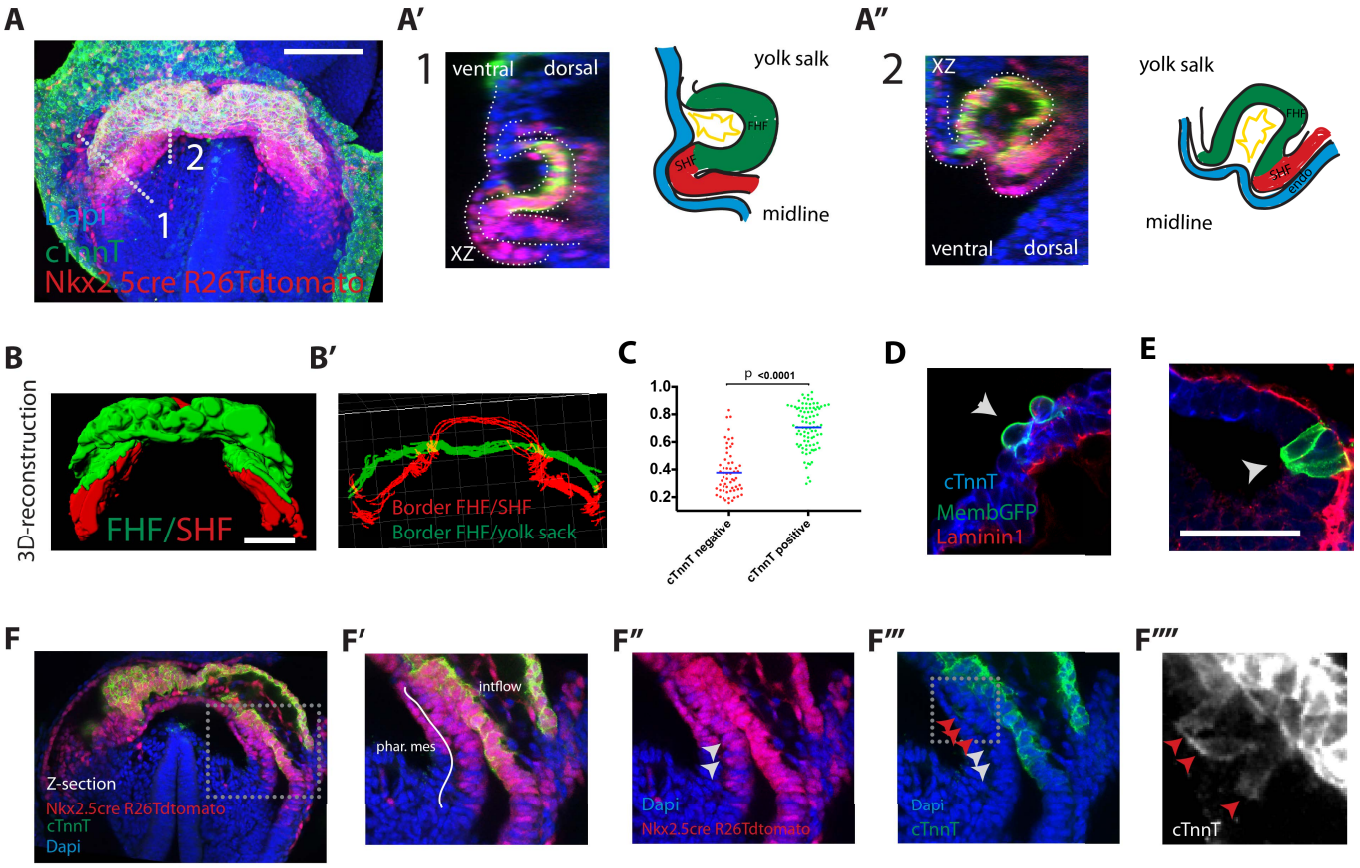

Figure 2. Visualisation of the boundary between FHF and SHF. (A-A'') Nkx2.5cre/+; R26tdtomato embryo immunostained for cTnnT (green) and Dapi (blue) showing cells of the Nkx2.5 lineage populating both the FHF and SHF. (A' and A'') Cross-sections in xz along the dotted lines 1 and 2 shown in (A), and corresponding schematics highlighting the endoderm (bleu), FHF (green), SHF (red) and endocardium (yellow). (B) 3D reconstruction of the FHF (green) and SHF (red); (B') 3D drawing of the border between the FHF and SHF (in red) and the FHF and yolk sack (in green) (based on the embryo shown in (A). For SHF rendering, the tdtomato+ splanchnic mesoderm was depicted. The FHF was rendered using the cTnnT signal. See also Video 3. (C) Quantification of the cell roundness (rnd) index of cardiomyocytes at HT stage on single optical sections. Black bars indicate mean. Rnd index for cTnnT+ (green) cells is 0.71 ± 0.16 and for cTnnT- (red) cells is 0.38 ± 0.16, mean ± SD, p value < 0.0001. (D-E) Membrane-GFP labelling of typical cTnnT+ FHF (D) and cTnnT-SHF (E) cells at longitudinal HT stage. Embryo is immunostained for cTnnT (blue), the basement membrane marker Laminin1 (red) and GFP (green). (F) Single optical section of the same embryo shown in (k). (F'-F''') Inset: red arrows point to cells localizing weak cTnnT signal and have columnar cell shape in the SHF. White arrows point to cTnnT-negative SHF cells. In all the embryos immunostained for cTnnT, the yolk sack signal is background. Scale bars: 100 µm except in (D-E): 50 µm.

Figure 2–source data 1.

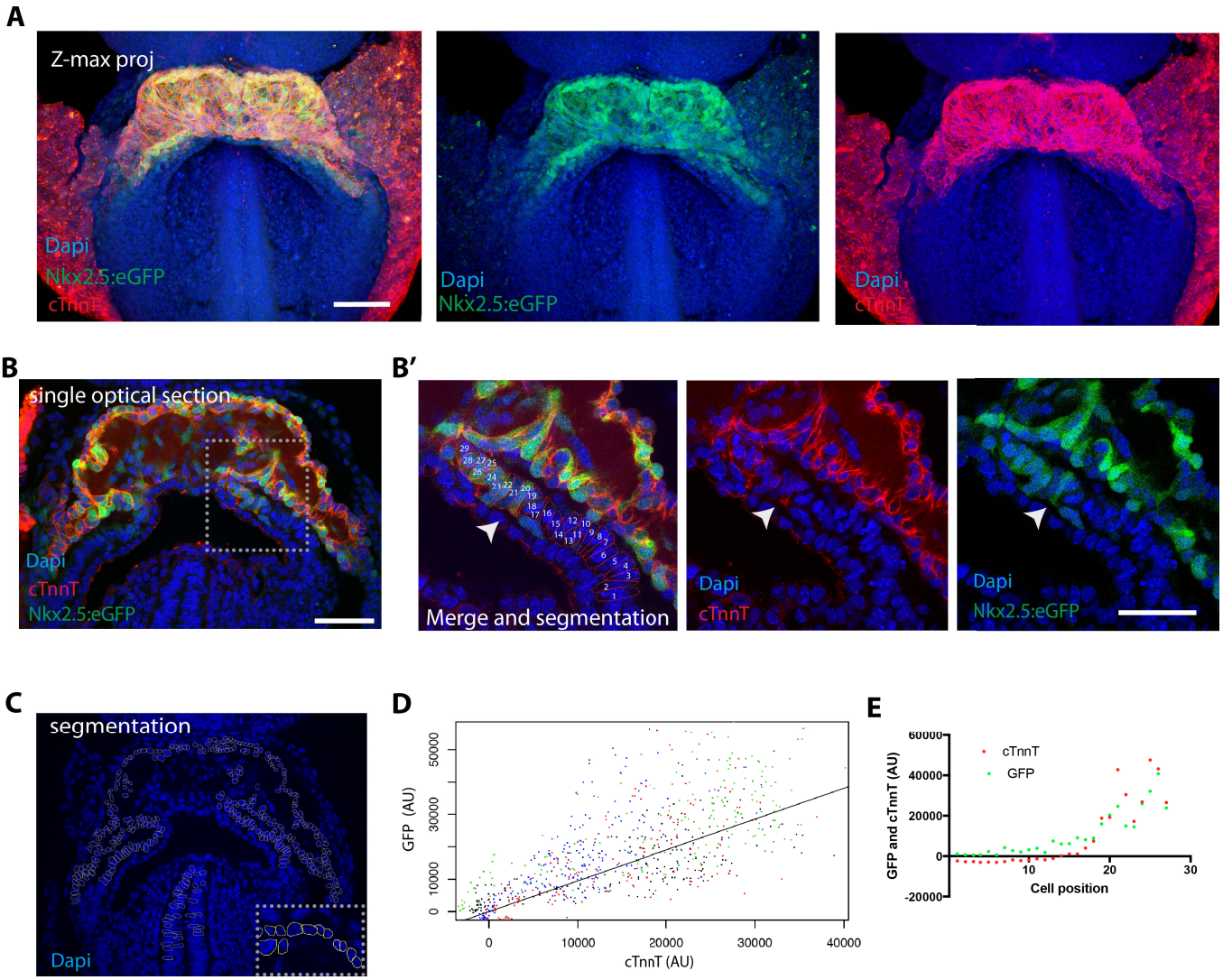

Figure 3. (A) z-maximum projection of an Nkx2.5eGFP embryo at transversal HT stage immunostained for cTnnT (red) and Dapi (blue) showing high GFP level in differentiated cardiomyocytes. (B) Single optical section of an Nkx2.5eGFP embryo at transversal HT stage immunostained for cTnnT (red) and Dapi (blue). (B') Inset in (B): arrow points the transition between cTnnT+ and cTnnT- domains, corresponding to FHF and SHF, respectively. Cells are manually segmented and labeled along the boundary from cTnnT-negative SHF to cTnnT-positive FHF. (C) Example of manual segmentation based on Dapi nuclei in cells located in the splanchnic mesoderm, myocardium and neural tube. (D) Linear mixed-effects model to find the relationship between the background substracted GFP and cTnnT levels adjusted by embryo (GFP=0.95*cTnnT, R2=0.81, p=2.2e-16) (n=762 cells analysed from 4 embryos). (E) GFP and cTnnT mean intensities measured within manually segmented cells along the boundary from cTnnT-negative SHF to cTnnT-positive FHF (B'). Scale bars: 100 µm.

Figure 3–Figure supplement 1. The Nkx.2.5eGFP and cTnnT labelling at different z-level.

Figure 3–Figure supplement 2. High GFP levels are detected in cTnnT-positive cells.

Figure 3–Figure supplement 3. Nkx2.5Cre genetic tracing labels both the FHF and SHF

Figure 3–source data 1.

2-photon live-imaging of early cardiac development in the mouse embryo

We next established a live-imaging method to dynamically characterize the formation of the HT in the mouse embryo (Figure 4A) (Chen et al., 2014). We adapted a previously reported culture system (Nonaka, 2009; Nonaka et al., 2002) in which the whole mouse embryo is immobilised by inserting the extraembryonic region in a holder (Figure 4C). After culture, embryos showed normal morphology, their hearts were beating and circulation was initiated (Figure 4D,E and Figure 4-figure supplement 1A and Video 4). This culture system in combination with multi-photon microscopy enabled to generate high-resolution 4D movies (Figure 3B and see Methods and Materials).

Imaging Mesp1cre/+; R26mtdtomato embryos allowed imaging the whole mesoderm (Saga et al., 1996; Saga et al., 1999) in 3D including all cardiac lineages from cc stage up to HT stage (Figure 4F,F' and Videos 5-6). It provided information on the formation of the endocardial lumen (Figure 4F") and on the anterior movement of the splanchnic mesoderm that is coincident to the folding of the cardiac crescent into an hemi-tube (white arrows in Figure 4F). Imaging Nkx2.5cre/+; R26mtdtomato/mGFP embryos, in which both precursors and differentiated cardiomyocytes are labelled, enabled to track cells during differentiation as they transit from a columnar to a round shape and start contracting (Figure 4G-G" and Videos 7-8).

We next tracked cardiac differentiation using the Nkx2.5eGFP live reporter. At E7/bud stage (see Figure 1-figure supplement 1 for staging criteria (Kirstie A. Lawson, 2016)), faint and scattered GFP signal is detected in proximity to the yolk sack, at the anterior border of the embryo (Figure 4-figure supplement 1A). At neural plate stage, just prior to the ventral folding of the embryo, the GFP signal remains weak but spreads to delineate a crescent in the anterior region of the embryo (Figure 4-figure supplement 1A and Video 9). From EHF, the GFP signal increases in intensity in correlation with the observation that cTnnT signal increases from this stage (Figure 4H, Figure 1C and Video 10). From transversal to open HT and closed HT stage, the GFP signal remains stable (Figure 4-figure supplement 1B,C and Video 11). We conclude that an increase in GFP level in the Nkx2.5eGFP transgenic reports cardiomyocyte differentiation. In addition, these results reveal the timing of the main phases of linear HT development; cc differentiation, formation of the open HT and dorsal closure (Figure 4I).

Live tracking of Cardiomyocyte differentiation in individual cells reveals cardiac crescent differentiation dynamics

We next sought to track the trajectories and differentiation of individual cardiac precursors within the entire cardiogenic region by 3D live-imaging. To this end, we used the RERT allele (Guerra et al., 2003), which provides ubiquitous tamoxifen-inducible Cre activity in combination with a Rosa26R-tdtomato reporter. We then titrated the tamoxifen dose for a labelling density that would allow single cell tracking during prolonged time-lapse analysis and combined this with the Nkx2.5eGFP reporter (see Methods and Materials). Typically, for each movie, we acquired z-slices every 3-5um achieving a total z-dimension of 200-300 µm -depending on the stage considered- and manually tracked in 3D for several hours an initial 50 to 100 cells per movie, which represents around 10% of the total number of cells present in the cc (de Boer et al., 2012).

We first tracked cells of the cardiac forming region from EHF stage –when cardiac precursors are undifferentiated– up to stages in which cardiomyocytes have differentiated in the cc but have not reached the transversal HT stage yet (Figure 5A and Figure 5-source data 1). During the onset of cardiac differentiation, the cardiac crescent folds ventrally and we found that the relative positions of the cardiac progenitors are maintained from the initial stage through the differentiated cc (Video 12). Relative cell positions therefore remain mostly coherent as the embryonic tissues undergo this initial global movement. Differentiation events are detected in some of the tracked cells by cell shape change from columnar to round and by the increase in GFP signal (see example in Figure 5B,D and Figure 5-source data 1). In contrast, other tracked cells remain in contact with the endoderm, retain their initial shape and show low GFP level throughout the movies. Next, in order to establish a fate map of the cardiac forming region at the EHF stage we tracked back in time the population of

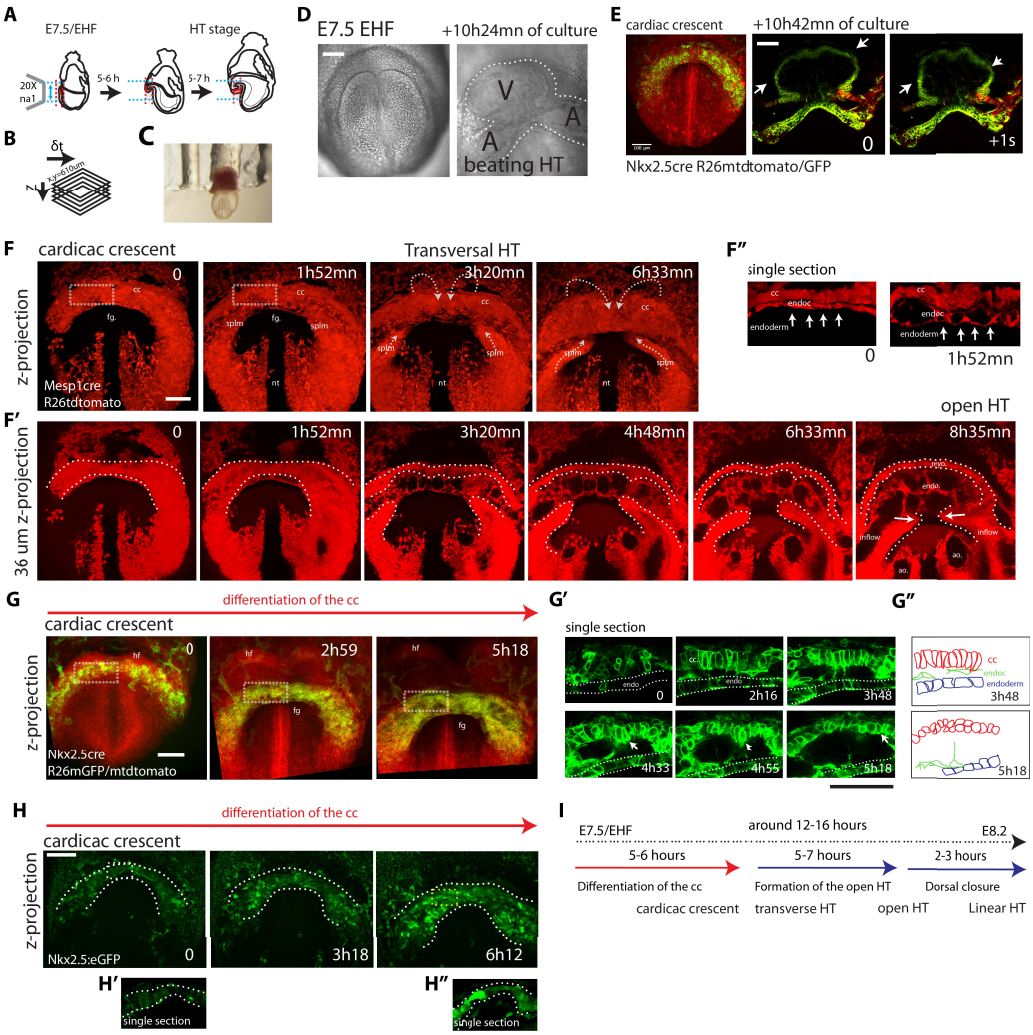

Figure 4. Live-imaging of cardiac differentiation and morphogenesis (A) Schematic of the set up for imaging live mouse embryos from EHF up to completion of HT formation. (B) Parameters xyzt during live-imaging. (C) An embryonic holder maintains the embryo still during live-imaging. (D-E) After over 10 hours of ex-vivo culture -inside the multi-photon chamber- the embryo has grown and the cardiac crescent transformed into a beating heart tube. Arrows in (E) point to the deformation of the heart ventricle during one heart beat cycle. See also Video 4. (F-F'') Time-lapse movie sequence of a Mesp1cre/+; R26tdtomato embryo –reporting whole mesoderm–, showing the transition from cardiac crescent stage to heart tube stage. Note that at the initial time point, the foregut pocket is already visible. Arrows indicate the major tissue movements visible (folding of the cardiac crescent, cranial movement of the splanchnic mesoderm). The differentiation of cardiomyocytes detaching from the endoderm is visible in (F'). White arrows point to the endocardium. The formation of the endocardial lumen in the transversal HT is visible in F'. By 8h35mn, the open HT is fully formed and beating regularly. Images are z-max projection of 84 sections covering 180 µm (F) and 9 sections covering 36 µm (F') acquired every 4 µm. See also Videos 5-6. (G-G'') (G) Time-lapse movie of an Nkx2.5cre/+; R26mtdtomato/mGFP embryo during the early stages of cardiac differentiation. Images are z-max projection of 87 sections acquired every 5 µm covering 437 µm. (G') shows in a single optical section how progenitors change in cell shape and move away from the endoderm during differentiation towards cardiomyocytes (from inset in (G)). (G'') Cartoon depicting the change in cell shape taking place during cardiac differentiation. See also Video 7. (H) Time-lapse movie sequences of Nkx2.5eGFP embryos, from cardiac crescent stage showing an increase in GFP level during the stages cardiomyocytes undergo differentiation. (H' and H'') Cardiomyocytes in single magnified optical sections. Images are z-max projection of 70 optical sections acquired every 6 µm covering 420 µm. See also Video 10. (I) Estimate of the timing between different heart tube development stages. Scale bars: 100 µm. fg: foregut cc: cardiac crescent, endoc: endocardium, ao: aorta, endo: endoderm, splm: splanchnic mesoderm, nt: neural tube

Figure 4–Figure supplement 1. Live-imaging of Nkx2.5eGFP reported line

Figure 4–Figure supplement 2. Embryos can be cultured and imaged under the 2-photon microscope for up to 24hours.

cells that showed high GFP intensity (top 50%) at the last time point of the movie (Figure 5F, H and Figure 5-source data 1) –since according to our previous analysis (Figure 3D)– these cells can reliably be assigned to cardiomyocytes. The initial location of the cells that increase their GFP level during tracking delineates a crescent-shaped domain at EHF stage (Figure 5H). Cells retaining lower GFP intensity level throughout the movie initially localise preferentially posteriorly and medially to this crescent. Most of the cells that have high GFP levels at the final time point have low GFP levels at the initial time point and sharply increase their GFP level over time (Figure 5E-G and Figure 5-source data 1). These results suggest that cardiomyocytes of the cc differentiate during 5-6 hours starting at the EHF stage, which is consistent with the onset of detectable cTnnT at that stage (Figure 1B and Figure 1-figure supplement 2A,A').

Cells in the cardiac mesoderm do divide during the observation time, so we identified cell division events and tracked the descendant cells. 43% of the tracked cells underwent one division during the 4-5 hour movies. To determine whether cell fate (differentiation versus progenitor) is lineage-allocated in the cardiogenic mesoderm at the EHF stage, we tracked GFP levels in dividing cells and their descendants. We found that most sister cell pairs show similar high or low GFP intensity levels at the end of the observation period (38 out of 39, Figure 5I, Figure 5- figure supplement 1A-D and Figure 5-source data 1). This observation suggests that commitment of cardiac precursors to differentiate is already established by the EHF stage and largely transmitted by lineage.

Cardiomyocyte differentiation is not detected during heart tube morphogenesis

We next studied cardiac differentiation dynamics during subsequent stages when the cc transforms into the HT by extensive morphogenesis. To do so, we tracked cells located in the splanchnic mesoderm in Nkx2.5-eGFP embryos at successive periods of around 3 hours covering the 5-7 hours during which the transversal HT transforms into the open HT (Figure 6A,B,E, Video 13 and Figure 4-source data 1). We also tracked cardiomyocytes in the forming HT. The HT starts to beat during the observation period, especially at the later stages, and therefore, in some cases, cardiomyocyte cell shape can be distorted in single optical sections (Figure 6F), however the GFP level could be determined. Anterior movement of the cells can be observed in the splanchnic mesoderm concomitant with the transformation of the transversal HT into the open HT (visible also in Video 5 and 11). We found that cells with high GFP level –differentiated cardiomyocytes– at the initial time points retain rather stable GFP levels (green tracks in Figure 6C,D, G and Figure 6-source data 1). In addition, all cells that initially showed low GFP levels did not increase GFP intensity during time-lapse, and cardiac differentiation was therefore not detectable (red tracks in Figure 6C,D).

To confirm the absence of detectable cardiac differentiation events during this period, we next focused on cells located at the boundary area where progenitors are located outside the HT. As expected, we observed in the movies low-GFP cells located adjacent to high-GFP cells in the boundary zone (Figure 6H). Those cells retain stable GFP levels throughout the tracking time and did not increase their GFP level (Figure 6I, boundary imaged 20 times in distinct locations and in 6 independent embryos).Importantly, they retain a columnar cell shape typical of weak cTnnT+ and cTnnT- columnar cells located at the boundary zone (see Figure 2F" and Figure 3B'). They also remain attached to endoderm and did not migrate into the HT. We confirmed this observation in longer time-lapse movies spanning 7 hours that covered the full transition period from transversal to open HT stage. Again, progenitors kept a strict boundary between with the differentiated cardiomyocytes of the HT throughout the entire time-lapse movie (Figure 7A-A'" and Video 14, boundary imaged 5 times in distinct locations and in 2 independent embryos). All together, these data suggest that during the transformation of the cc into the dorsally open HT no cardiomyocytes are added to the HT from the SHF. These observations suggest two distinct phases of early HT formation: a first phase of differentiation of the FHF into the cc, lasting around 5 hours, and a second phase of HT morphogenesis in which the SHF progenitors remain undifferentiated, lasting around 7 hours.

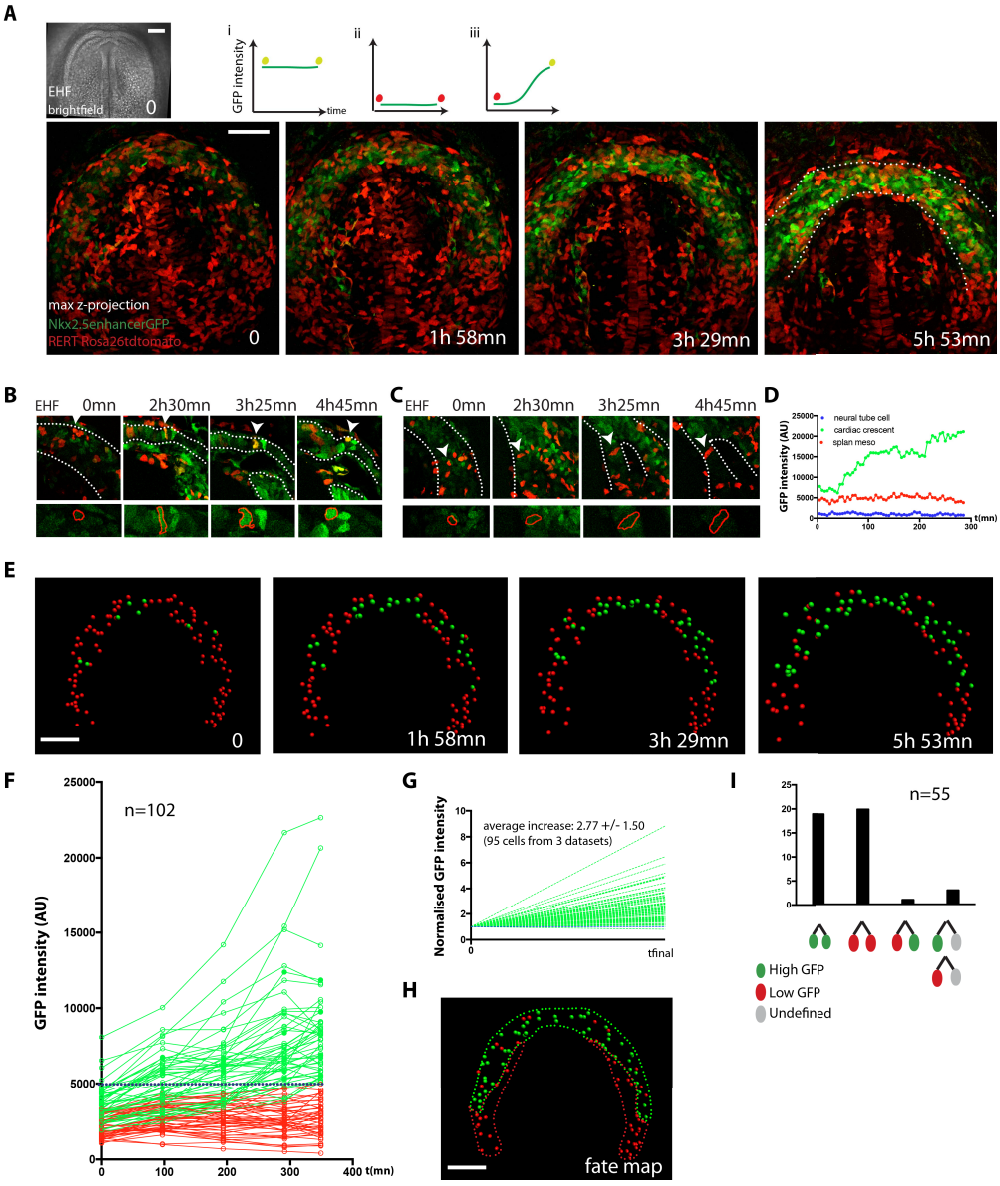

Figure 5. Live-imaging of cardiac differentiation at cellular resolution. (A) Time course of an RERT; R26tdtomato; Nkx2.5eGFP embryo during stages when cc differentiation takes place -from EHF onwards-. Images are Z-maximum projection of 76 sections acquired every 3 µm covering 228 µm. A brighfield image of the EHF embryo at the initial time point is also shown. (i, ii and iii) Rationale of the expected evolution of GFP expression: since tracks carry information on reporter expression, if a cell acquires a high level of GFP, we predict that it is committed to differentiate. See also Video 12. (B-D) Examples of time-lapse movies (B and C) and quantification of the GFP level (D) increasing in a single cardiomyocyte during differentiation (B) or remaining low in a cell located in the splanchnic mesoderm (C). A neural tube cell has been additionally quantified (blue). Images are single optical sections. (E) Time course of individual cells tracked in movie (A). Cells with GFP levels above the median intensity value of all cells at the end time point are represented as green spheres and cells with lower GFP levels are shown as red spheres. (F) GFP level through time. Blue dotted line: median value (5249 a.u.). GFP level for each tracked cell was measured at five successive time points. Cell divisions are not represented for simplicity. (G) Normalised GFP level showing an increase in GFP level in the green classified cells. Average increase: 2,77 folds ± 1.50, mean ± SD, n=95 cells from 3 independent datasets. (H) The differentiation fates (green, cell that differentiates, red, cell that does not) of mesodermal cells were mapped onto the initial cardiac crescent at EHF stage. (I) Progenitor descendant cells share differentiation fate. Lineages of dividing progenitors (n=55 from 3 independent datasets) were identified during early stages of cardiac differentiation. Two daughter cells are defined as sharing the same fate if their GFP intensity levels do not differ by more 1.5 fold and/or remain both above or below the threshold value defined. Scale bars: 100 µm.

Figure 5–Figure supplement 1. Cells divide during cardiac differentiation.

Figure 5–source data 1.

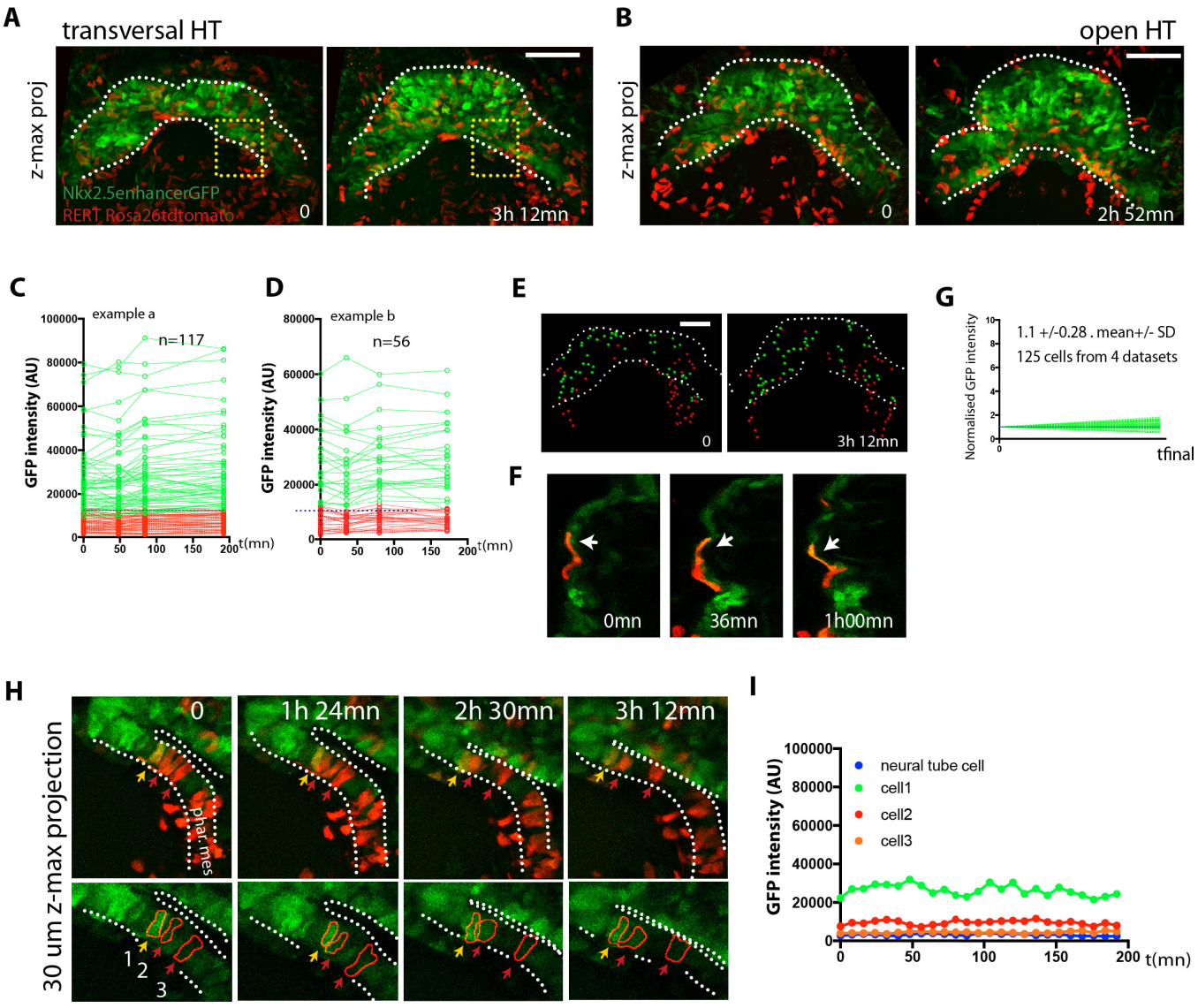

Figure 6. No cardiac differentiation is detected during early HT morphogenesis (A-B) Initial and final time points of two time-lapse movie of RERT; R26tdtomato/+; Nkx2.5eGFP embryos covering the transformation of the transversal HT into the open HT. Images are z-maximum projection of 44 sections acquired every 5 µm covering 220 µm in (A) and of 46 sections acquired every 6 µm covering 276 µm in (B). See also Video 13. (C, D) GFP levels over time of the cells tracked in (A, B). GFP level for each tracked cell was measured at four successive time points. Green tracks represent cardiomyocytes with GFP intensity above the median intensity value of all the tracked cells at the last time point, while red tracks represent cells with lower GFP level. Blue dotted line represents the median intensity value (10748 a.u. in (C) and 12248a.u. in (D)). Note that when cells divide, only one of the two daughter cells was represented for simplicity. (E) Distribution of the tracked cells from the time-lapse movie shown in (A). Red and Green classified cells are represented as spheres. (F) Example of red-labelled cardiomyocytes tracked in the beating HT ventricle. (G) Normalised progression of GFP level in green classified cells showing stable GFP levels. Data collected from 125 tracked cells from four independent movies of 2h52 to 3h12mn periods. Average increase: 1,1 folds ± 0.28, mean ± SD. (H-I) (H) Example extracted from the movie in (A, yellow inset) of red-labelled cells in the boundary zone between undifferentiated and differentiated cells. (I) Quantification of GFP level through time of the three segmented cells shown in (H). Cells have stable GFP level and do not differentiate. Images are z-maximum projections of 6 sections acquired every 5 µm covering 30 µm. Scale bars: 100 µm.

Figure 6–source data 1.

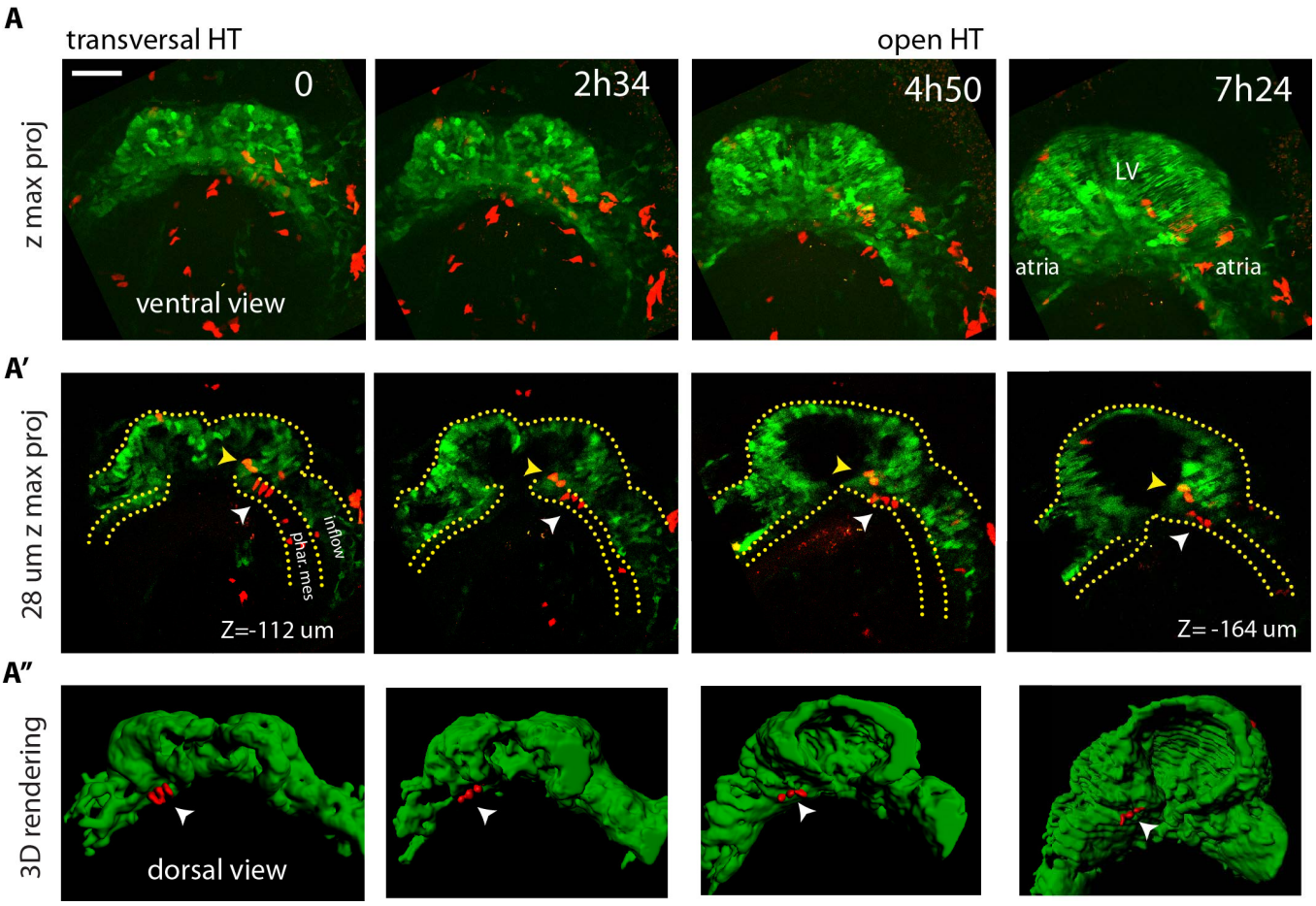

Figure 7. (A-A") Time-lapse movie of an RERT; R26tdtomato; Nkx2.5eGFP embryo during the stages at which the transversal HT transforms into an open HT, showing cells located in the splanchnic mesoderm (white arrows in A' and A"), respecting the boundary with the HT (yellow arrows in J' show two cells located in the HT). Lower doses of tamoxifen have been injected in order to label only few cells in red. Images are z-maximum projection of 74 sections (A) acquired every 4 µm covering 296 µm and (A') 7 sections covering 28 µm. (A") 3D reconstruction based of the Nkx2.5eGFP signal (green) and red-labelled cells located in the splanchnic mesoderm. See also Video 14. Scale bars:100 µm

Imaging the Isl1-expressing cell lineage confirms absence of cardiac progenitor differentiation during early heart tube morphogenesis

The LIM domain transcription factor Islet1 (Isl1) is a cardiac progenitor marker. Its expression is transient in the precursors of the cc, while it remains expressed in SHF progenitors for an extended period (Brade et al., 2007; Prall et al., 2007) (Yuan and Schoenwolf, 2000). Cells of the Isl1 lineage detected with Cre reporters therefore contribute only scarcely to the cc, while extensively to the SHF and its derivatives (Cai et al., 2003; Ma et al., 2008). To test these observations in live imaging, we combined Nkx2.5-eGFP with tracing of the Isl1 cell lineage using the Ils1cre/+ driver and the R26tdtomato/tdtomato reporter. We found that tdtomato-labelling is first detectable in scarce isolated cells of the GFP+ cc when the cc folds ventrally and differentiates (from t=2h36m to t=4h in Figure 8A,B). A dense tdtomato-labelling appears instead in the GFP-low cells of the splanchnic mesoderm (from t=2h24m to t=4h in Figure 8A and C and Video 15), as well as in the endoderm and endocardium (not shown). Consistently with previous reports (Cai et al., 2003), Cre-recombination detected in live analysis occurs at low frequency in the cc and at high frequency in the SHF.

Once the cc is formed, if cells of the SHF would continuously differentiate, then regions of the forming heart tube contributed by the SHF precursors should be densely co-labelled by both the GFP and tdtomato fluorophore. Live imaging shows instead that tdtomato+ cells establish a boundary with GFP+ cells, indicating again no signs of differentiation of SHF precursors during the observation period (Figure 8A,C and Videos 16). Multi-photon imaging however doesn't allow to image unambiguously all cells located deep inside the live tissue at the final stages recorded, because of limited depth penetration and light scattering resulting in low signal to noise ratio. The prospective outflow track in particular is located deep in the embryo (Figure 8- figure supplement 1A-A", at around -200 µm depth, see next section) and it is therefore challenging to accurately track GFP levels there. To overcome these limitations, we fixed the embryos after completion of the live-imaging experiments, immunostained those embryos against cTnnT and imaged them after clearing by confocal microscopy. No domains containing predominantly double-labelled cells were detected, indicating that progenitors located in the SHF did not undergo differentiation in the boundary zone from cc to open HT stage (Figure 7D). These results are consistent with our single cell tracking analysis and confirm that the SHF does not differentiate during linear HT morphogenesis.

Cardiac differentiation is detected during the late stages of HT development

We next wanted to determine when cardiac progenitors located in the SHF start to differentiate. We fixed Nkx2.5-eGFP; Ils1cre/+; R26tdtomato/+ embryos at different stages from cc up to heart looping (n=10) and assessed the appearance of GFP and tdtomato double-positive domains in the HT. In agreement with our previous observations, we found that SHF cells do not differentiate up to the open HT stage, when the dorsal seam of the heart is still open. In contrast, massive appearance of double positive cells is observed subsequently in the fully closed HT reinforcing our previous interpretation (Zaffran et al., 2004) (Laugwitz et al., 2005) (Moretti et al., 2006) (Figure 8E, F and Videos 17-18). At this stage the primordium of the RV has been added to the OFT and is fully composed of double-positive cells. The dorsal seam of the HT is also densely populated by double-positive cells, indicating a contribution of precursors from the SHF to the cardiomyocyte population that finalizes the dorsal closure of the linear HT.

Discussion

Here, we established a whole-embryo live-imaging method based on multiphoton microscopy that allows us whole-tissue tracking at cellular resolution. By combining various genetic tracing tools, we labelled progenitor and differentiated cardiomyocytes and performed 3D cell tracking over time combined with 3D reconstruction of the HT at multiple stages. We report three distinct temporal phases of HT formation (Figure 9). During the first phase, the cc differentiates rapidly and morphogenesis, in terms of changes in the relative position of cells is minimal. During the

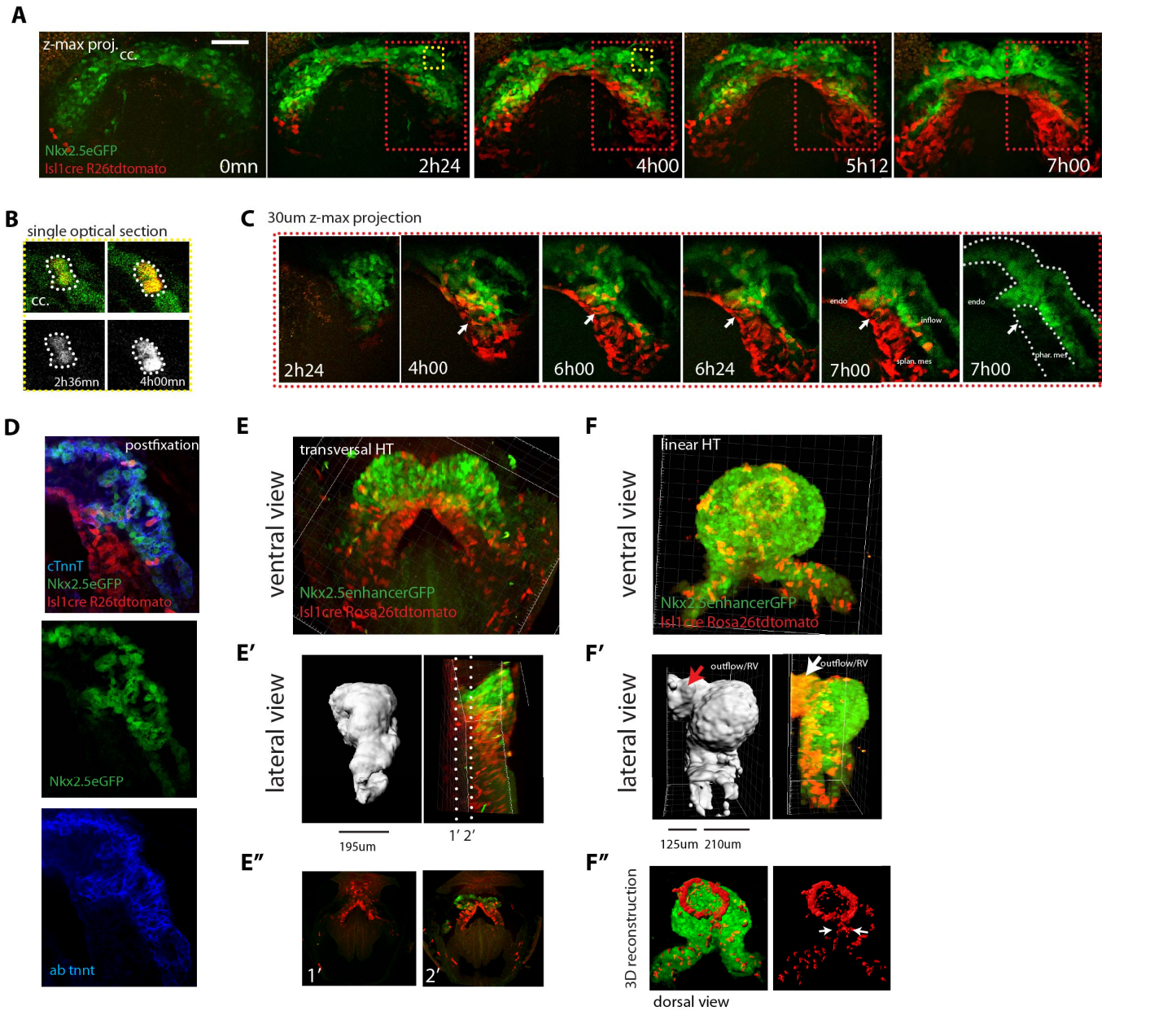

Figure 8. Analysis of Isl1- expressing cells during early heart development. (A) Time-lapse movie sequences of an Ils1cre/+; R26tdtomato/+; Nkx2.5eGFP embryo showing that the Rosa26 locus recombines at a higher frequency in the splanchnic mesoderm compared to the FHF (n=3 movies from cc up to open HT stage). (B) Yellow inset from (A). Two cells of the Isl1 lineage located in the cc increase their tdtomato level over time. (C) Red inset in (A); increase of the tdtomato intensity in the splanchnic mesoderm over time. Arrow shows the boundary between SHF and FHF and points to a single cell in the SHF that retains a low level of GFP and an elongated cell shape. Images are z-maximum projection of 45 sections acquired every 5um and covering 225 µm in (A) and of 6 sections covering 30 µm in (C). Interval between frames: 6min. See also Videos 15-16. (D) Same embryo as in (A) post-fixed and immunostained against cTnnT after live-imaging, showing that the red cells located in the splanchnic mesoderm are undifferentiated. (E, F) Ils1cre/+; R26tdtomato/+; Nkx2.5eGFP embryos showing no contribution of the Isl1 lineage to the differentiated HT (E-E") but contributing robustly to the outflow tract and dorsal aspect of the linear HT (F- F"). The presence of double-positive cells in these areas reveals the differentiation of Isl1 lineage cells into cardiomyocytes (F, F"). Images are 74 and 134 optical sections acquired every 2.5 µm and covering 195 µm and 335 µm, respectively. In (F, F') only the double-positive cells located in the linear HT are shown, while the tdtomato+ progenitors, located outside the linear HT are not shown. Lateral views are shown in (E', F') including 3D reconstruction. (E") Cross-sections xy along the dotted lines shown in (E'). Dorsal views are shown in (F") including the 3D reconstruction of the tdtomato+ cells located in the linear HT. White arrows show the dorsal regions of the linear HT. endo : endoderm, splan meso: splanchnic mesoderm. Scale bars: 100 µm.

Figure 8–Figure supplement 1. GFP level in deeper z level cannot be accurately quantified.

second phase, differentiation is not detected and morphogenetic remodelling gives rise to a dorsally open HT. During the third phase, cardiac precursor recruitment and differentiation resumes, contributing to the formation of the RV and the dorsal closure of the HT. Our results support the early establishment of distinct FHF and SHF cell populations and show that the morphogenetic changes that transform the cc into a HT largely take place in the absence of cardiac precursor differentiation. These observations indicate tissue-level coordination of differentiation and morphogenesis during early cardiogenesis in the mouse.

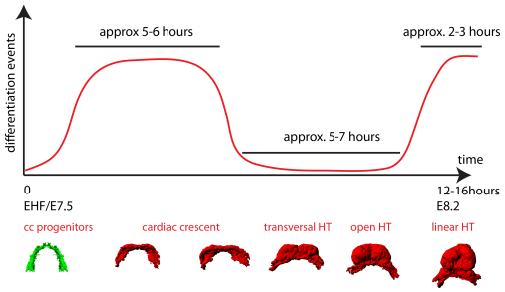

Figure 9. A model of cardiomyocyte differentiation dynamics during early heart development. We propose that two distinct phases of cardiomyocyte differentiation take place during early heart development. At EHF, the cc differentiates and starts folding. Cardiomyocytes round up and become contractile while the cardiac progenitors located in the splanchnic mesoderm remain undifferentiated. Subsequently, the cc. undergoes further morphogenesis to transform into a HT, initially open dorsally and no cardiomyocyte differentiation is detected during this transformation. Finally, cardiac differentiation resumes contributing new cardiomyocytes from the splanchnic mesoderm to the outflow track, (the prospective RV), and the dorsal closure of the HT.

We show in addition similarities in the differentiation dynamics of SHF precursors and cardiomyocytes contributing to the dorsal regions of the linear HT (Meilhac et al., 2004b). The dorsal aspect of the linear HT gives rise to the inner curvature of the looped heart, which generates non-chamber myocardium contributing to atrioventricular canal and conduction system. Our results suggest that the late recruitment of progenitors in the dorsal HT contributes to the specification of cardiomyocytes in this region of the HT as non-chamber myocardium, while the ventral domains of the linear HT will become specialized as ventricular chamber myocardium (Christoffels et al., 2000).

Prospective clonal analyses showed that the FHF and SHF are specified at different time points during gastrulation and have distinct molecular signatures (Devine et al., 2014; Lescroart et al., 2014). Here, by direct cell lineage tracing coupled with differentiation reporting, we suggest that FHF and SHF precursors are largely lineage allocated in the cardiogenic region prior to differentiation. Further studies will be required, however, to assess how genes differentially expressed in the FHF and SHF contribute to the regulation of the two distinct differentiation schedules described here. Environmental clues could also control the sequential differentiation of FHF and SHF precursors. The Wnt and BMP pathways are well known regulators of cardiac differentiation (Ai et al., 2007; Jain et al., 2015; Klaus et al., 2007; Kwon et al., 2007; Marvin et al., 2001; Qyang et al., 2007; Tirosh-Finkel et al., 2010; Ueno et al., 2007) and specific mechanisms affecting these pathways could be operating during the formation the HT, whereby the differentiation pathways could be temporally restrained.

In zebrafish, elegant experiments using a cardiac myosin light chain reporter line similarly address the temporal order of cardiac differentiation in live embryos using high resolution imaging(de Pater et al., 2009; Liu and Stainier, 2012). Two distinct phases of cardiomyocyte differentiation separated in time were also observed. During a first phase, cardiomyocytes were recruited in the linear HT. During a second phase, a late cardiogenic population of cardiomyocytes was added at the arterial pole of the HT. This study did not report, however, an arrest of cardiac differentiation during the morphogenesis of the initial HT as we do observe in Mouse. Instead, cardiac differentiation seems to be continuous and extensively overlaps with morphogenetic reorganisations in zebrafish. It would be therefore of interest to further address the morphogenetic and evolutionary implications of these differences.

Our study applies for the first time whole-embryo live analysis of cardiac development at tissue level and with cellular resolution. We expect that extending this experimental approach to additional

aspects of embryonic development will allow to further uncover unexpected and novel mechanisms of organogenesis. In addition, limited attention had been paid so far to the temporal dynamics of differentiation during embryonic development, yet it is an essential aspect of organogenesis (Gogendeau et al., 2015; Parchem et al., 2015; Yang et al., 2015). Here we show the relevance of regulation of differentiation timing during heart tube formation. Further understanding of the molecular and cellular mechanisms underlying these phenomena will help us expanding pools of cardiac progenitors in vitro or directing them towards differentiation.

Methods and Materials

Mouse Strains

The following mouse lines were used: Mesp1cre (Saga et al., 1999), Isl1cre (Cai et al., 2003), Nkx2.5cre (Stanley et al., 2002), Rosa26tdtomato (Madisen et al., 2010), ROSA26mTmG (Muzumdar et al., 2007), Nkx2.5eGFP (Wu et al., 2006), CreERT2 (RERT) (Guerra et al., 2003) and C57BL/6. Mice were genotyped as previously described. All animal procedures were approved by the CNIC Animal Experimentation Ethics Committee, by the Community of Madrid (Ref. PROEX 220/15) and conformed to EU Directive 2010/63EU and Recommendation 2007/526/EC regarding the protection of animals used for experimental and other scientific purposes, enforced in Spanish law under Real Decreto 1201/2005.

Immunostaining and Imaging

Embryos dissected in Dulbecco's modified Eagle's medium (DMEM, Invitrogen) were fixed overnight in 2% PFA at 4 °C, then permeabilised in PBST (PBS containing 0.1% Triton X-100) and blocked (5% goat serum). Embryos were incubated overnight at 4 °C with antibodies diluted in PBST: mouse anti-cTnnT (1:250, MS-295 Thermo Scientific), rabbit anti-PH3 (1:250, 06-570 Millipore) and rabbit anti-Laminin1 (1:500, Sigma). After washing in freshly prepared PBST at 4C, embryos were incubated with secondary antibodies (Molecular Probes) coupled to 488, 549 or 649 fluorophores as required at 1:250 and DAPI at 1:500 (Molecular Probes) overnight at 4 °C. Before imaging, embryos were washed in PBST at room temperature and cleared with focus clear (Cell Explorer) to enhance the transparency of the embryo. Confocal images were obtained on a SP8 Leica confocal microscope with a 20X oil objective (0.7 NA) at a 1024 × 1024 pixel dimension with a z-step of 2-4 µm. Embryos were systematically imaged throughout the entire heart tube from top to bottom.

3D Reconstruction and Volumetric Measurement

For 3D rendering, fluorescent signal in confocal z-stacks was first segmented by setting intensity thresholds using the trainable Weka segmentation tool plugin available in Fiji (Arganda-Carreras et al., 2017; Schindelin et al., 2012). The resulting z-stacks were then corrected manually on a slide-by-slide basis to eliminate segmentation mistakes. In case of the cTnnT immunofluorescence images (Figure 1), background signal from the yolk sack was manually masked. Volume of the cTnnT positive myocardium was then computed by multiplying the total segmented area by the z-stack interval using custom Fiji macro. In the Nkx2.5cre/+; R26tdtomato and Nkx2.5eGFP embryos, fluorophore signal present in the endothelium, endocardium and endoderm cells was manually masked prior to segmentation (Figure 2B , Figure 6A"). For 3D visualisation of the 3D segmented image stacks, Imaris software (Bitplane) was used.

Embryo Culture and Multiphoton Live-Imaging

Embryos were dissected at E7.5 in pre-equilibrated DMEM supplemented with 10% foetal bovine serum, 25 mM HEPES-NaOH (pH 7.2), penicillin (50uml21) and streptomycin (50 mg ml21). Embryos were staged on the basis of morphological criteria (supplementary Figure 1) (Downs and Davies, 1993; Kirstie A. Lawson, 2016), and those between the bud and early somitogenesis stages were used for culture and time-lapse imaging. To track the early phase of cardiac differentiation and

subsequent phase of morphogenesis, we used embryo at EHF and transversal HT stage respectively. Embryos were cultured in 50% fresh rat serum, 48% DMEM without phenol red, 1% N-2 neuronal growth supplement (100X, Invitrogen 17502-048) and 1percent B-27 supplement (50X Thermo Fisher Scientist 17504044) filter sterilised through a 0.2 mm filter. To hold the embryo in position during time-lapse acquisition, we made special plastic holders with holes of different diameters (0.5-3 mm) to ensure a good fit of the embryos similarly to the traps developed by Nonaka et al. (Nonaka, 2009; Nonaka et al., 2002). Embryos were mounted with their anterior side facing up. To avoid evaporation, the medium was covered with mineral oil (Sigma-Aldrich; M8410). Before starting the time-lapse acquisition, the embryos were first pre-cultured for at least 2 hours in the microscopy culture set up. The morphology of the embryo was then carefully monitored and if the embryos appeared unhealthy or rotate and move, they were discarded, otherwise, time-lapse acquisition was proceed. For the acquisition, we used the Zeiss LSM780 2-photon microscope equipped with a 5% CO2 incubator and a heating chamber maintaining 37 °C. The objective lens used was a 20X (NA=1) deeping objectives that has a long working distance for imaging mouse embryos and tissues. MaiTai laser line 1000 nm was used for 2-channel 2-photon imaging. Acquisition was done using Zen software (Zeiss). Typical image settings were: output power: 250mW, pixel dwell time: 7us, line averaging: 2 and image dimension: 610x610um (1024x1024 pixels). To maximize the chance of covering the entire heart tube during long term time lapse movies, we included, at the starting point, 150-200 µm of imaging space in z over the top of the embryo.

Cell labelling and 3D tracking and GFP Intensity Measurement

For labelling of single cells, Tamoxifen was administered by oral gavage (2-4 mg/mL) in RERT/Rosa26R-tdtomato at E7. We then tracked single tdtomato-labelled cells located within the cardiogenic mesoderm -excluding endothelial, pericardial and endodermal cells- and measured their GFP intensity over time. To track cells manually in 4D stacks, the MTrackJ Fiji plugin (Meijering et al., 2012) was used. A local square cursor (25x25 pixels) on the cell of interest snaps according to a bright centroid feature on a slice-by-slice basis. Only tracks lasting for the entire length of the movie were kept. When an ambiguity arises in the tracking, from one time point to the next, the track was discarded. Tracks split at cell divisions. A cell division event is normally clearly distinguishable over at least 2 time points. In case one of the two daughter cells is not tractable, the other daughter cell is still tracked. Each tracks is assigned an ID number and a excel files with all the tracks coordinates in x, y, z and t was generated. Coordinates of each tracks were converted into 8-bit 4D image using a custom Fiji macro in which each cells was represented by a sphere of specific pixel intensity, from 1 to 255, while pixels corresponding to background were set to zero. The 4D images were then opened with Imaris to perform visualization of the 3D trajectories of each cells using spots tool, where each object were identified according to pixel intensity. GFP intensity measurement is performed by segmentation of cell shape. A Gaussian filter whose radius is adjusted to the typical size of a cell was first applied, followed by a Laplacian filter. The resulting 32 bits image was next converted to a mask by thresholding. When objects were touching each other, a watershed on the binary mask and manual corrections was applied. Each segmented cells was checked and tracked manually for accuracy. In Figure 2E nuclei segmentation was performed manually. The mean GFP signal intensity of the segmented objects was then measured using the “analyse particle” tool in Fiji. To quantify GFP level through time of tracked cells, four to five successive time points were arbitrarily chosen in each dataset (Figure 5F, Figure 6C,D and Figure 5-figure supplement 1C) except in Figure 5D and Figure 6I, where GFP intensity level was measured in every time point. Background intensities were measured in neural tube cells, which are known to be negative for GFP and cTnnT. Tables containing ID tracked number and GFP intensities were generated and plotted using Prism statistical software.

Statistical Analysis

For comparisons of two groups, a Man-Whitney U-test was used using Prism statistical software. To find a correlation between GFP and cTnnT levels of 0.8 with an alpha-level of 0.05 and a power of 0.2 at least 10 cells per embryo were required (Figure 3D and Figure 3-figure supplement 2C). Many more cells were computed for each experiments. The linear fit was done using lm function from the R statistical software (www.r-project.org).

Acknowledgments

We thank the CNIC Microscopy unit for help with the live confocal analysis, Fatima Sanchez Cabo for help with the statistical analyses and Florencia Cavodeassi, Miguel Manzanares, Brian Laruy and members of the Torres lab for helpful comments on the manuscript. This work was supported by grants BFU2015-71519-P and RD16/0011/0019 (ISCIII) from the Spanish Ministry of Economy, Industry and Competitiveness (MEIC). KI was supported by a Human Frontiers Science Program (LT000609/2015) and EMBO (ATL1275-2014) postdoctoral fellowships. The CNIC is supported by the Spanish MEIC and the Pro CNIC Foundation, and is a Severo Ochoa Center of Excellence (MINECO award SEV-2015-0505). The authors declare no conflicts of interest.

Author Contributions

KI and MT conceived the project, KI performed the experiments and analysed the data, ST provided technical help, KI and MT wrote the manuscript

References

Abu-Issa, R. (2014). Heart fields: spatial polarity and temporal dynamics. Anat Rec (Hoboken) 297, 175-182.

Abu-Issa, R., Waldo, K., and Kirby, M.L. (2004). Heart fields: one, two or more? Dev Biol 272, 281-285.

Ai, D., Fu, X., Wang, J., Lu, M.F., Chen, L., Baldini, A., Klein, W.H., and Martin, J.F. (2007). Canonical Wnt signaling functions in second heart field to promote right ventricular growth. Proc Natl Acad Sci U S A 104, 9319-9324.

Arganda-Carreras, I., Kaynig, V., Rueden, C., Eliceiri, K.W., Schindelin, J., Cardona, A., and Seung, H.S. (2017). Trainable Weka Segmentation: a machine learning tool for microscopy pixel classification. Bioinformatics.

Biben, C., Weber, R., Kesteven, S., Stanley, E., McDonald, L., Elliott, D.A., Barnett, L., Koentgen, F., Robb, L., Feneley, M., et al. (2000). Cardiac septal and valvular dysmorphogenesis in mice heterozygous for mutations in the homeobox gene Nkx2-5. Circ Res 87, 888-895.

Brade, T., Gessert, S., Kuhl, M., and Pandur, P. (2007). The amphibian second heart field: Xenopus islet-1 is required for cardiovascular development. Dev Biol 311, 297-310.

Buckingham, M., Meilhac, S., and Zaffran, S. (2005). Building the mammalian heart from two sources of myocardial cells. Nat Rev Genet 6, 826-835.

Cai, C.L., Liang, X., Shi, Y., Chu, P.H., Pfaff, S.L., Chen, J., and Evans, S. (2003). Isl1 identifies a cardiac progenitor population that proliferates prior to differentiation and contributes a majority of cells to the heart. Dev Cell 5, 877-889.

Chen, C.M., Miranda, A.M., Bub, G., and Srinivas, S. (2014). Detecting cardiac contractile activity in the early mouse embryo using multiple modalities. Front Physiol 5, 508.

Christoffels, V.M., Habets, P.E., Franco, D., Campione, M., de Jong, F., Lamers, W.H., Bao, Z.Z., Palmer, S., Biben, C., Harvey, R.P., et al. (2000). Chamber formation and morphogenesis in the developing mammalian heart. Dev Biol 223, 266-278.

Christoffels, V.M., Mommersteeg, M.T., Trowe, M.O., Prall, O.W., de Gier-de Vries, C., Soufan, A.T., Bussen, M., Schuster-Gossler, K., Harvey, R.P., Moorman, A.F., et al. (2006). Formation of the

venous pole of the heart from an Nkx2-5-negative precursor population requires Tbx18. Circ Res 98, 1555-1563.

de Boer, B.A., van den Berg, G., de Boer, P.A., Moorman, A.F., and Ruijter, J.M. (2012). Growth of the developing mouse heart: an interactive qualitative and quantitative 3D atlas. Dev Biol 368, 203-213.

de Pater, E., Clijsters, L., Marques, S.R., Lin, Y.F., Garavito-Aguilar, Z.V., Yelon, D., and Bakkers, J. (2009). Distinct phases of cardiomyocyte differentiation regulate growth of the zebrafish heart. Development 136, 1633-1641.

Devine, W.P., Wythe, J.D., George, M., Koshiba-Takeuchi, K., and Bruneau, B.G. (2014). Early patterning and specification of cardiac progenitors in gastrulating mesoderm. Elife 3.

Downs, K.M., and Davies, T. (1993). Staging of gastrulating mouse embryos by morphological landmarks in the dissecting microscope. Development 118, 1255-1266.

Evans, S.M., Yelon, D., Conlon, F.L., and Kirby, M.L. (2010). Myocardial lineage development. Circ Res 107, 1428-1444. Francou, A., Saint-Michel, E., Mesbah, K., and Kelly, R.G. (2014). TBX1 regulates epithelial polarity and dynamic basal filopodia in the second heart field. Development 141, 4320-4331.

Gogendeau, D., Siudeja, K., Gambarotto, D., Pennetier, C., Bardin, A.J., and Basto, R. (2015). Aneuploidy causes premature differentiation of neural and intestinal stem cells. Nat Commun 6, 8894.

Guerra, C., Mijimolle, N., Dhawahir, A., Dubus, P., Barradas, M., Serrano, M., Campuzano, V., and Barbacid, M. (2003). Tumor induction by an endogenous K-ras oncogene is highly dependent on cellular context. Cancer Cell 4, 111-120.

Jain, R., Li, D., Gupta, M., Manderfield, L.J., Ifkovits, J.L., Wang, Q., Liu, F., Liu, Y., Poleshko, A., Padmanabhan, A., et al. (2015). HEART DEVELOPMENT. Integration of Bmp and Wnt signaling by Hopx specifies commitment of cardiomyoblasts. Science 348, aaa6071.

Kelly, R.G., Brown, N.A., and Buckingham, M.E. (2001). The arterial pole of the mouse heart forms from Fgf10-expressing cells in pharyngeal mesoderm. Dev Cell 1, 435-440.

Kelly, R.G., Buckingham, M.E., and Moorman, A.F. (2014). Heart fields and cardiac morphogenesis. Cold Spring Harb Perspect Med 4.

Kirstie A. Lawson, V.W. (2016). A Revised Staging of Mouse Development Before Organogenesis. Kaufman's Atlas of Mouse Development Supplement.

Klaus, A., Saga, Y., Taketo, M.M., Tzahor, E., and Birchmeier, W. (2007). Distinct roles of Wnt/beta-catenin and Bmp signaling during early cardiogenesis. Proc Natl Acad Sci U S A 104, 18531-18536.

Kwon, C., Arnold, J., Hsiao, E.C., Taketo, M.M., Conklin, B.R., and Srivastava, D. (2007). Canonical Wnt signaling is a positive regulator of mammalian cardiac progenitors. Proc Natl Acad Sci U S A 104, 10894-10899.

Laugwitz, K.L., Moretti, A., Lam, J., Gruber, P., Chen, Y., Woodard, S., Lin, L.Z., Cai, C.L., Lu, M.M., Reth, M., et al. (2005). Postnatal isl1+ cardioblasts enter fully differentiated cardiomyocyte lineages. Nature 433, 647-653.

Lescroart, F., Chabab, S., Lin, X., Rulands, S., Paulissen, C., Rodolosse, A., Auer, H., Achouri, Y., Dubois, C., Bondue, A., et al. (2014). Early lineage restriction in temporally distinct populations of Mesp1 progenitors during mammalian heart development. Nat Cell Biol 16, 829-840.

Lien, C.L., Wu, C., Mercer, B., Webb, R., Richardson, J.A., and Olson, E.N. (1999). Control of early cardiac-specific transcription of Nkx2-5 by a GATA-dependent enhancer. Development 126, 75-84.

Linask, K.K., Knudsen, K.A., and Gui, Y.H. (1997). N-cadherin-catenin interaction: necessary component of cardiac cell compartmentalization during early vertebrate heart development. Dev Biol 185, 148-164.

Liu, J., and Stainier, D.Y. (2012). Zebrafish in the study of early cardiac development. Circ Res 110, 870-874.

Ma, Q., Zhou, B., and Pu, W.T. (2008). Reassessment of Isl1 and Nkx2-5 cardiac fate maps using a Gata4-based reporter of Cre activity. Dev Biol 323, 98-104.

Madisen, L., Zwingman, T.A., Sunkin, S.M., Oh, S.W., Zariwala, H.A., Gu, H., Ng, L.L., Palmiter, R.D., Hawrylycz, M.J., Jones, A.R., et al. (2010). A robust and high-throughput Cre reporting and characterization system for the whole mouse brain. Nat Neurosci 13, 133-140.

Marvin, M.J., Di Rocco, G., Gardiner, A., Bush, S.M., and Lassar, A.B. (2001). Inhibition of Wnt activity induces heart formation from posterior mesoderm. Genes Dev 15, 316-327.

Meijering, E., Dzyubachyk, O., and Smal, I. (2012). Methods for cell and particle tracking. Methods Enzymol 504, 183-200.

Meilhac, S.M., Esner, M., Kelly, R.G., Nicolas, J.F., and Buckingham, M.E. (2004a). The clonal origin of myocardial cells in different regions of the embryonic mouse heart. Dev Cell 6, 685-698.

Meilhac, S.M., Esner, M., Kerszberg, M., Moss, J.E., and Buckingham, M.E. (2004b). Oriented clonal cell growth in the developing mouse myocardium underlies cardiac morphogenesis. J Cell Biol 164, 97-109.

Mjaatvedt, C.H., Nakaoka, T., Moreno-Rodriguez, R., Norris, R.A., Kern, M.J., Eisenberg, C.A., Turner, D., and Markwald, R.R. (2001). The outflow tract of the heart is recruited from a novel heart-forming field. Dev Biol 238, 97-109.

Moorman, A.F., Christoffels, V.M., Anderson, R.H., and van den Hoff, M.J. (2007). The heart-forming fields: one or multiple? Philos Trans R Soc Lond B Biol Sci 362, 1257-1265.

Moretti, A., Caron, L., Nakano, A., Lam, J.T., Bernshausen, A., Chen, Y., Qyang, Y.,Bu, L., Sasaki, M., Martin-Puig, S., et al. (2006). Multipotent embryonic isl1+ progenitor cells lead to cardiac, smooth muscle, and endothelial cell diversification. Cell 127, 1151-1165.

Muzumdar, M.D., Tasic, B., Miyamichi, K., Li, L., and Luo, L. (2007). A global double-fluorescent Cre reporter mouse. Genesis 45, 593-605.

Nonaka, S. (2009). Modification of mouse nodal flow by applying artificial flow. Methods Cell Biol 91, 287-297.

Nonaka, S., Shiratori, H., Saijoh, Y., and Hamada, H. (2002). Determination of left-right patterning of the mouse embryo by artificial nodal flow. Nature 418, 96-99.

Parchem, R.J., Moore, N., Fish, J.L., Parchem, J.G., Braga, T.T., Shenoy, A., Oldham, M.C., Rubenstein, J.L., Schneider, R.A., and Blelloch, R. (2015). miR-302 Is Required for Timing of Neural Differentiation, Neural Tube Closure, and Embryonic Viability. Cell Rep 12, 760-773.

Prall, O.W., Menon, M.K., Solloway, M.J., Watanabe, Y., Zaffran, S., Bajolle, F., Biben, C., McBride, J.J., Robertson, B.R., Chaulet, H., et al. (2007). An Nkx2-5/Bmp2/Smad1 negative feedback loop controls heart progenitor specification and proliferation. Cell 128, 947-959.

Qyang, Y., Martin-Puig, S., Chiravuri, M., Chen, S., Xu, H., Bu, L., Jiang, X., Lin, L., Granger, A., Moretti, A., et al. (2007). The renewal and differentiation of Isl1+ cardiovascular progenitors are controlled by a Wnt/beta-catenin pathway. Cell Stem Cell 1, 165-179.

Ramsbottom, S.A., Sharma, V., Rhee, H.J., Eley, L., Phillips, H.M., Rigby, H.F., Dean, C., Chaudhry, B., and Henderson, D.J. (2014). Vangl2-regulated polarisation of second heart field-derived cells is required for outflow tract lengthening during cardiac development. PLoS Genet 10, e1004871.

Saga, Y., Hata, N., Kobayashi, S., Magnuson, T., Seldin, M.F., and Taketo, M.M. (1996). MesP1: a novel basic helix-loop-helix protein expressed in the nascent mesodermal cells during mouse gastrulation. Development 122, 2769-2778.

Saga, Y., Miyagawa-Tomita, S., Takagi, A., Kitajima, S., Miyazaki, J., and Inoue, T. (1999). MesP1 is expressed in the heart precursor cells and required for the formation of a single heart tube. Development 126, 3437-3447.

Schindelin, J., Arganda-Carreras, I., Frise, E., Kaynig, V., Longair, M., Pietzsch, T., Preibisch, S., Rueden, C., Saalfeld, S., Schmid, B., et al. (2012). Fiji: an open-source platform for biological-image analysis. Nat Methods 9, 676-682.

Sinha, T., Wang, B., Evans, S., Wynshaw-Boris, A., and Wang, J. (2012). Disheveled mediated planar cell polarity signaling is required in the second heart field lineage for outflow tract morphogenesis. Dev Biol 370, 135-144.

Spater, D., Abramczuk, M.K., Buac, K., Zangi, L., Stachel, M.W., Clarke, J., Sahara, M., Ludwig, A., and Chien, K.R. (2013). A HCN4+ cardiomyogenic progenitor derived from the first heart field and human pluripotent stem cells. Nat Cell Biol 15, 1098-1106.

Stanley, E.G., Biben, C., Elefanty, A., Barnett, L., Koentgen, F., Robb, L., and Harvey, R.P. (2002). Efficient Cre-mediated deletion in cardiac progenitor cells conferred by a 3'UTR-ires-Cre allele of the homeobox gene Nkx2-5. Int J Dev Biol 46, 431-439.

Tirosh-Finkel, L., Zeisel, A., Brodt-Ivenshitz, M., Shamai, A., Yao, Z., Seger, R., Domany, E., and Tzahor, E. (2010). BMP-mediated inhibition of FGF signaling promotes cardiomyocyte differentiation of anterior heart field progenitors. Development 137, 2989-3000.

Tyser, R.C., Miranda, A.M., Chen, C.M., Davidson, S.M., Srinivas, S., and Riley, P.R. (2016). Calcium handling precedes cardiac differentiation to initiate the first heartbeat. Elife 5.

Ueno, S., Weidinger, G., Osugi, T., Kohn, A.D., Golob, J.L., Pabon, L., Reinecke, H., Moon, R.T., and Murry, C.E. (2007). Biphasic role for Wnt/beta-catenin signaling in cardiac specification in zebrafish and embryonic stem cells. Proc Natl Acad Sci U S A 104, 9685-9690.

Waldo, K.L., Hutson, M.R., Ward, C.C., Zdanowicz, M., Stadt, H.A., Kumiski, D., Abu-Issa, R., and Kirby, M.L. (2005). Secondary heart field contributes myocardium and smooth muscle to the arterial pole of the developing heart. Dev Biol 281, 78-90.

Wu, S.M., Fujiwara, Y., Cibulsky, S.M., Clapham, D.E., Lien, C.L., Schultheiss, T.M., and Orkin, S.H. (2006). Developmental origin of a bipotential myocardial and smooth muscle cell precursor in the mammalian heart. Cell 127, 1137-1150.

Yang, S.L., Yang, M., Herrlinger, S., Liang, C., Lai, F., and Chen, J.F. (2015). MiR-302/367 regulate neural progenitor proliferation, differentiation timing, and survival in neurulation. Dev Biol 408, 140-150.

Yuan, S., and Schoenwolf, G.C. (2000). Islet-1 marks the early heart rudiments and is asymmetrically expressed during early rotation of the foregut in the chick embryo. Anat Rec 260, 204-207.

Zaffran, S., Kelly, R.G., Meilhac, S.M., Buckingham, M.E., and Brown, N.A. (2004). Right ventricular myocardium derives from the anterior heart field. Circ Res 95, 261-268.

Videos

- Video 1: 3D reconstruction of the cardiac crescent at EHF stage, based on Nkx2.5cre R26tdtomato signal. Related to Figure1A.
- Video 2: 3D reconstruction of Mouse HT formation, based on embryos immunostained for cTnnT. Five representative stages are represented. Related to Figure 1C-G.
- Video 3: 3D reconstruction of the FHF (green) and SHF (red). Based on Nkx2.5cre R26tdtomato embryos immunostained for cTnnT. The border between cTnnT-negative and cTnnT-positive cells can be visualised at the interface between the red and green domains. Related to Figure 2B.
- Video 4: z-max projection of an Nkx.25crecre/+; R26mG/mt embryo at cc stage and time-lapse movie of the same embryo after 10h42mn of ex-vivo culture. Images are single optical sections and acquired every 1s (ss) (representative analysis from 3 mouses). Related to Figure 4E.
- Video 5: Time-lapse movie of a Mesp1cre/+; R26tdtomato embryo from cc up to open HT stage (h:mm:ss) (representative analysis from 4 mouses). Related to Figure 4F.
- Video 6: Same embryo as in Video 5. Images are z-max projection of 9 sections acquired every 4um covering 36um (h:mm:ss) and allows visualisation of the inside of the cardiac lumen during HT formation. Related to Figure 4F'.
- Video 7: Time-lapse movie of a an Nkx.25crecre/+; R26mG/mt embryo (h:mm:ss) (representative analysis from 2 mouses). Related to Figure 4G-G'.
- Video 8: Brightfield time-lapse movie of a wt embryo, from cc stage showing the differentiation, contractility of the cardiomyocytes, and formation of the cardiac lumen. Images are acquired every 1mn (h:mm:ss) (representative analysis from 2 mouses).

- Video 9: Time-lapse movie sequences of Nkx2.5eGFP embryos from Early Bud/E7.5 stage (h:mm:ss) (representative analysis from 2 mouses). Related to Figure 4-figure supplement 1A.
- Video 10: Time-lapse movie sequences of Nkx2.5eGFP embryos from cc to Hemi-tube stage (h:mm:ss) (representative analysis from 3 mouses). Related to Figure 4H.
- Video 11: Time-lapse movie sequences of Nkx2.5eGFP embryos from transversal HT to open HT stage (h:mm:ss) (representative analysis from 3 mouses). Related to Figure 4-figure supplement 1B.
- Video 12: Cell tracks in 3D represented with Imaris during stages cardiac differentiation takes place -from EHF onwards-. Cells are represented as green spheres if their GFP level is increasing and goes above a threshold value defined as the median intensity value of all the tracked cells at the last time point; and as red spheres when it remains below (h:mm:ss) (representative analysis from 3 mouses). Related to Figure 5A.
- Video 13: Cell tracks in 3D represented with Imaris during stages the open HT forms. Cells are represented as green spheres if their GFP level are above a threshold value defined as the median intensity value of all the tracked cells at the last time point; and as red spheres when they remains below (h:mm:ss) (representative analysis from 4 mouses). Related to Figure 6A.
- Video 14: Time-lapse movie of an RNApolIICrert/+; R26tdtomato; Nkx2.5eGFP embryo during the stages at which the transversal HT transforms into a open HT (h:mm:ss). (Latter half) 3D reconstruction at three time points based of the Nkx2.5eGFP signal (green) and red-labeled cells located in the splanchnic mesoderm. Related to Figure 7A.
- Video 15: Time-lapse movie of an Isl1Cre-/+; R26tdtomato; Nkx2.5eGFP embryo (h:mm:ss) (representative analysis from 3 mouses). (representative analysis from 2 mouses) Related to Figure 8A.
- Video 16: Same embryo shown in Video 14 zoomed in at the level of the splanchnic mesoderm (h:mm:ss). Related to Figure 8C.
- Video 17: 3D rendering of an Isl1Cret/+; R26tdtomato; Nkx2.5eGFP embryo at transversal HT stage. Related to Figure 8E.
- Video 18: 3D rendering of an Isl1Cret/+; R26tdtomato; Nkx2.5eGFP embryo at linear HT stage. Related to Figure 8F.

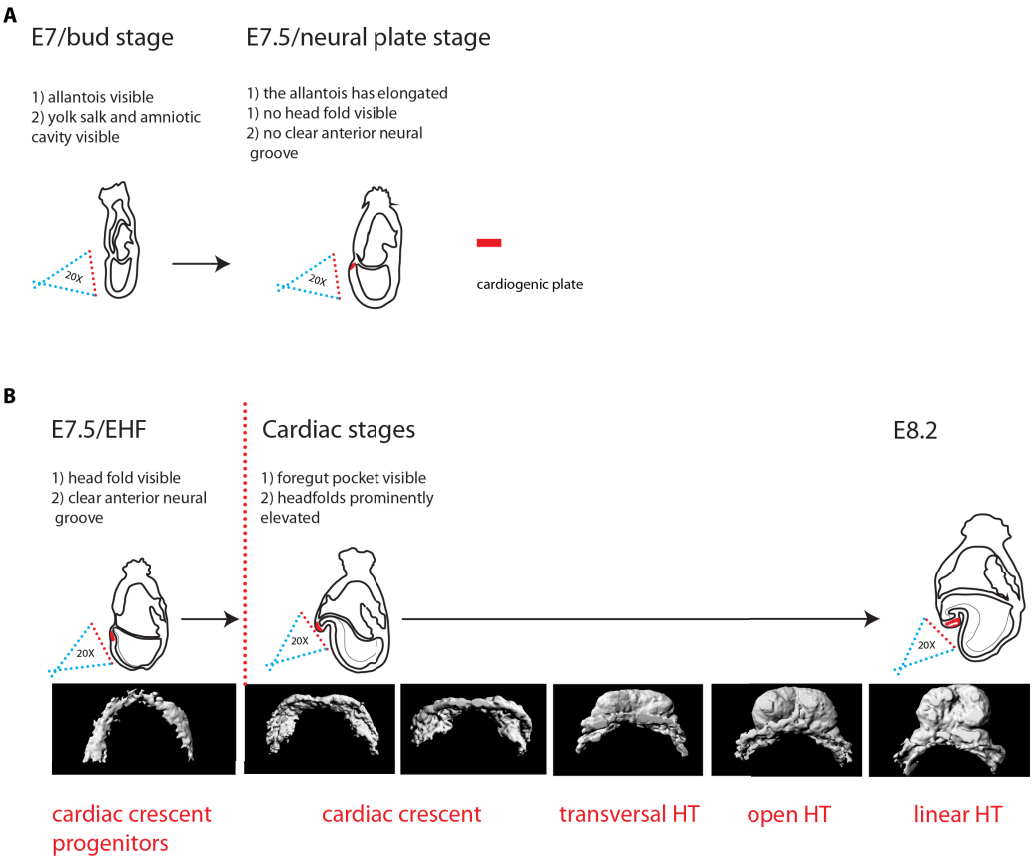

Figure 1–Figure supplement 1. Criteria for staging Embryos. We determined the developmental stage of embryos based on morphological landmark(Downs and Davies, 1993; Kirstie A. Lawson, 2016). (A) At bud stage/E7, a small allantois bud is visible. At neural pate stage/E7.5, the allantois is larger and project into the yolk sack cavity. The anterior neuroectoderm is enlarged. (B) At EHF/E7.5, the neural plate starts to form the head fold. During somitogenesis, a clearly visible foregut pocket appears and the head folds are located dorsally and anteriorly to the cardiac primordium. The cc has differentiated. It transforms successively into the transveral HT, the open HT and the linear HT closed dorsally and a prominent outflow/RV formed.

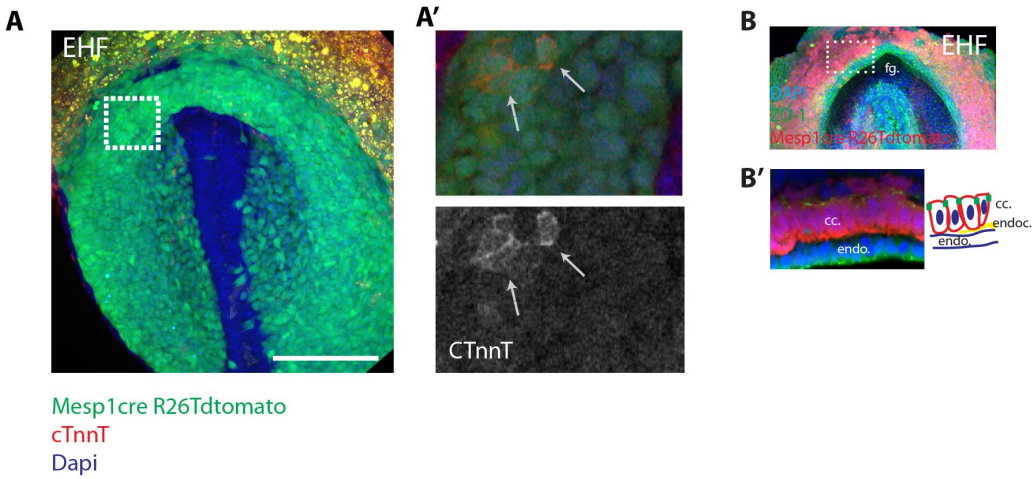

Figure 1–Figure supplement 2. Faint cTnnT signal starts to be detected at EHF stage in apico-basally polarised cc cells. (A) Mesp1cre/+; R26tdtomato embryo at EHF stage -labeling the mesoderm (green)- immunostained against cTnnT (red) and Dapi (blue). Note that the embryo is at a slightly more advanced developmental stage than those shown in (Figure 1B) because the foregut pocket is more invaginated. (A') White inset in (A). Faint cTnnT signal (red) in few mesodermal cells (arrows) can be detected. (B-B') Mesp1cre/+; R26tdtomato embryo showing the mesoderm in red and immunostained against the tight junction component zona-occludens-1 (ZO-1) (green) and Dapi (blue). The cc cells (as seen in transversal sections) have an AB polarised epithelial morphology. Scale bars: 150 µm

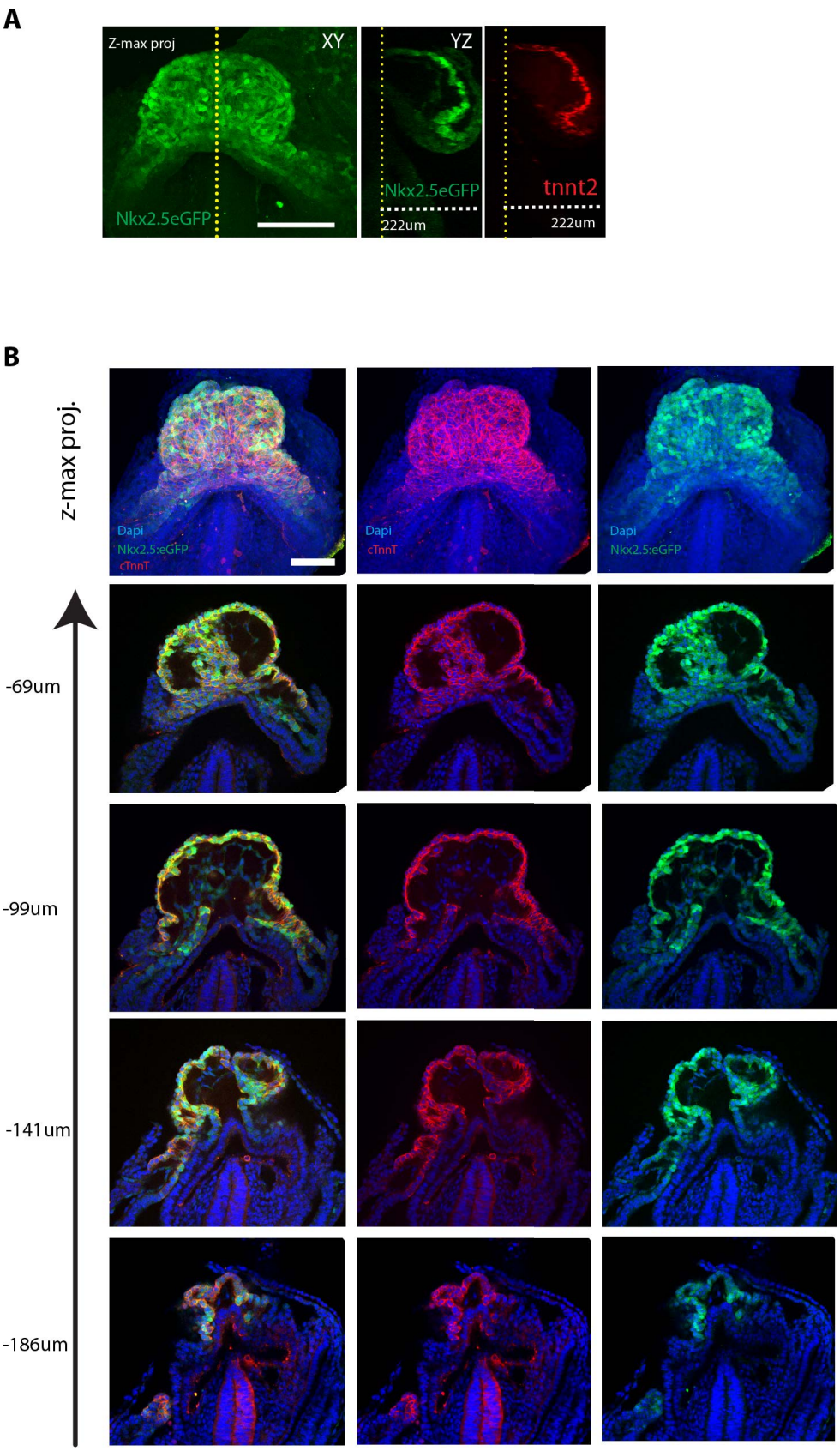

Figure 3–Figure supplement 1. The Nkx.2.5eGFP and cTnnT labelling at different z-level. (A) z-maximum projection and yz view of a Nkx2.5-eGFP embryo immunostained against cTnnT showing overlap between eGFP signal and cTnnT localisation in the z dimension. (B) z-maximum projection and optical sections at different z-level of an Nkx2.5eGFP embryo, immunostained for cTnnT (red) and Dapi (blue), showing overlapping expression of GFP and cTnnT signal. Scale bars: 100 µm.

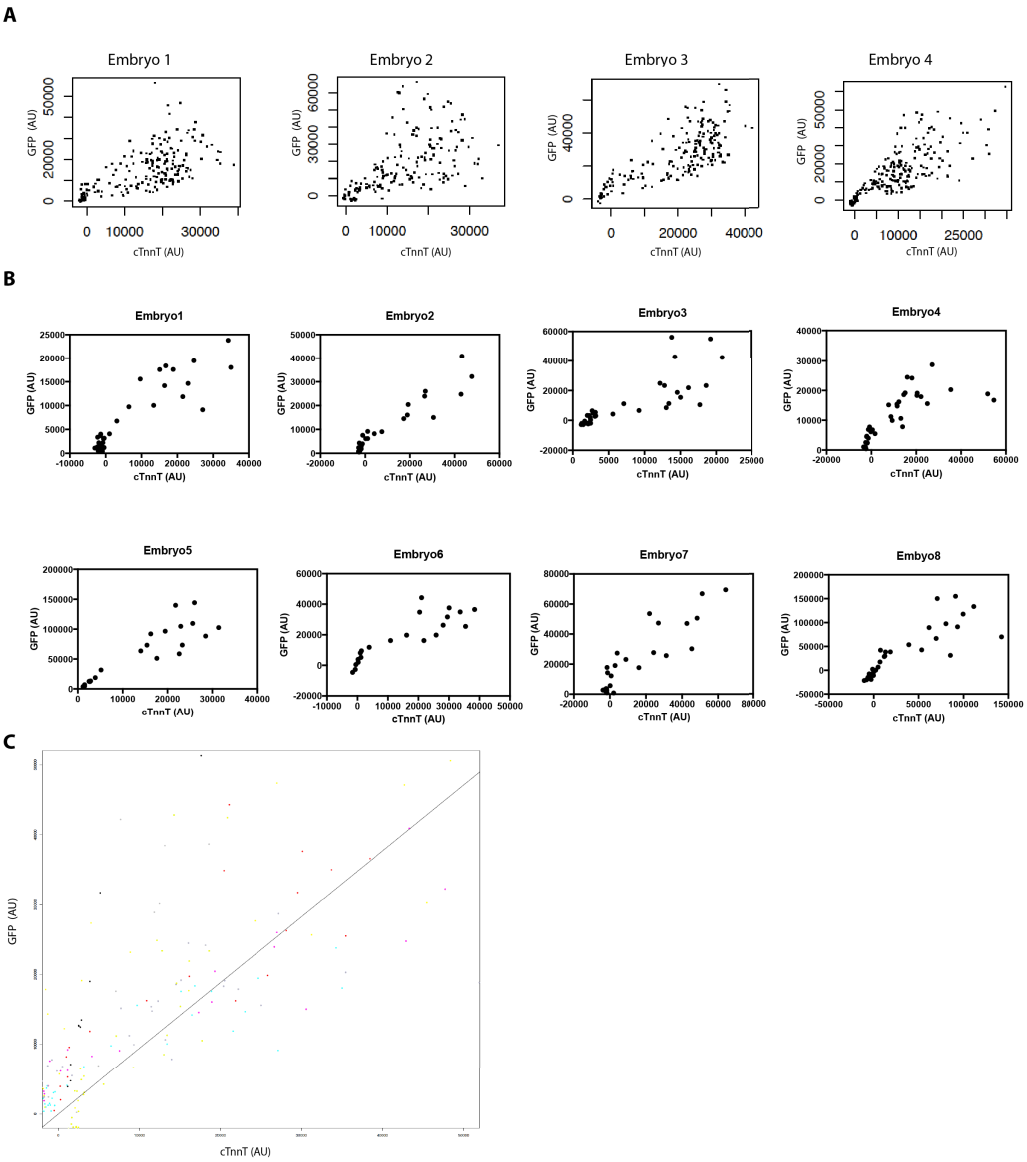

Figure 3–Figure supplement 2. High GFP levels are detected in cTnnT-positive cells. (A,B) Normalized GFP and cTnnT mean level for single segmented cell (A) located in the FHF and SHF and (B) located at the boundary zone between the FHF and SHF (n=130 cells analysed from 8 embryos). (C) Linear mixed-effects model to find the relationship between the background substracted GFP and cTnnT levels adjusted by embryo for cell located at the boundary between the FHF and SHF (GFP=0.94*cTnnT, R2=0.77, p<2.2e-16). Each dot represents a single segmented cell. Cells are being considered positive for cTnnT when their mean intensity value is above 0. Note that small GFP signal can be detected in the cTnnT-negative SHF cells. Scale bars: 100 μm.

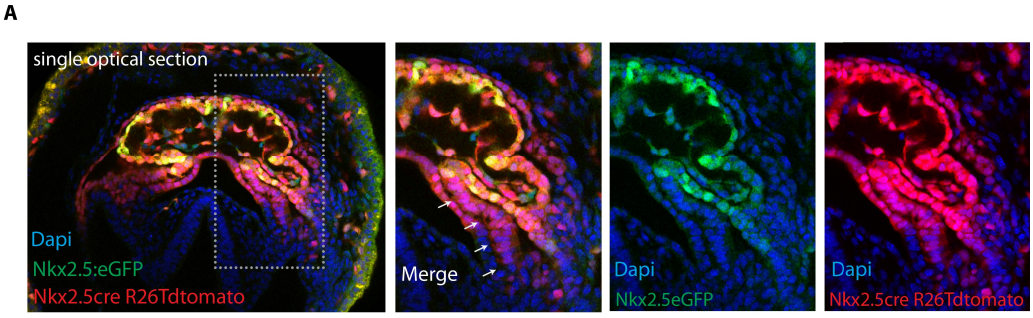

Figure 3–Figure supplement 3. Nkx2.5Cre genetic tracing labels both the FHF and SHF (A) The GFP expression of the Nkx2.5-eGFP reporter does not fully overlap with tdtomato expression pattern in Nkx2.5cre/+; R26tdtomato/+; Nkx2.5eGFP embryos at the level of the splanchnic mesoderm/SHF. Scale bars: 100 µm.

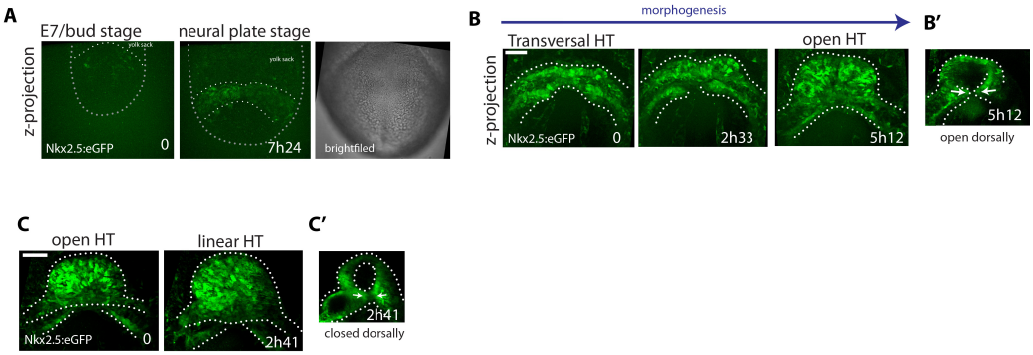

Figure 4–Figure supplement 1. Live-imaging of Nkx2.5eGFP reporter line. (A-D) Time-lapse movie sequences of Nkx2.5eGFP embryos from Early Bud (A), transversal HT (B) and open HT stage (C). Images are z-max projection of 75 sections acquired every 14 µm covering 300 µm in (A), 55 sections acquired every 6 µm covering 330 µm in (B) and 59 sections acquired every 5 µm covering 295 µm in (D). (B' and C'): z-max projection covering 132 µm (C') and 60 µm (D') showing the dorsal opening and the dorsal closure of the HT at the last time points. See also Videos 9 and 11.

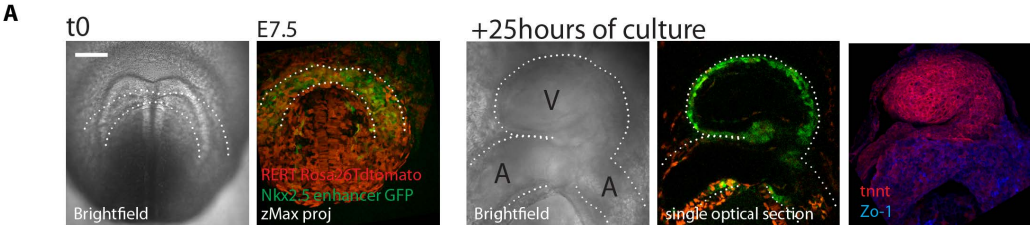

Figure 4–Figure supplement 2. Embryos can be cultured and imaged under the 2-photon microscope for up to 24hours.(A) RERT; R26tdtomato; Nkx2.5eGFP embryo. Starting culture at E7.5, by the end of the 25 hours ex-vivo culture, the HT has formed and looped (experiment repeated 3 times independantly). The embryo was subsequently fixed and immunostained for cTnnT (red) and ZO-1 (blue). V: prospective left ventricle, A: prospective atria. Scale bars: 100 µm

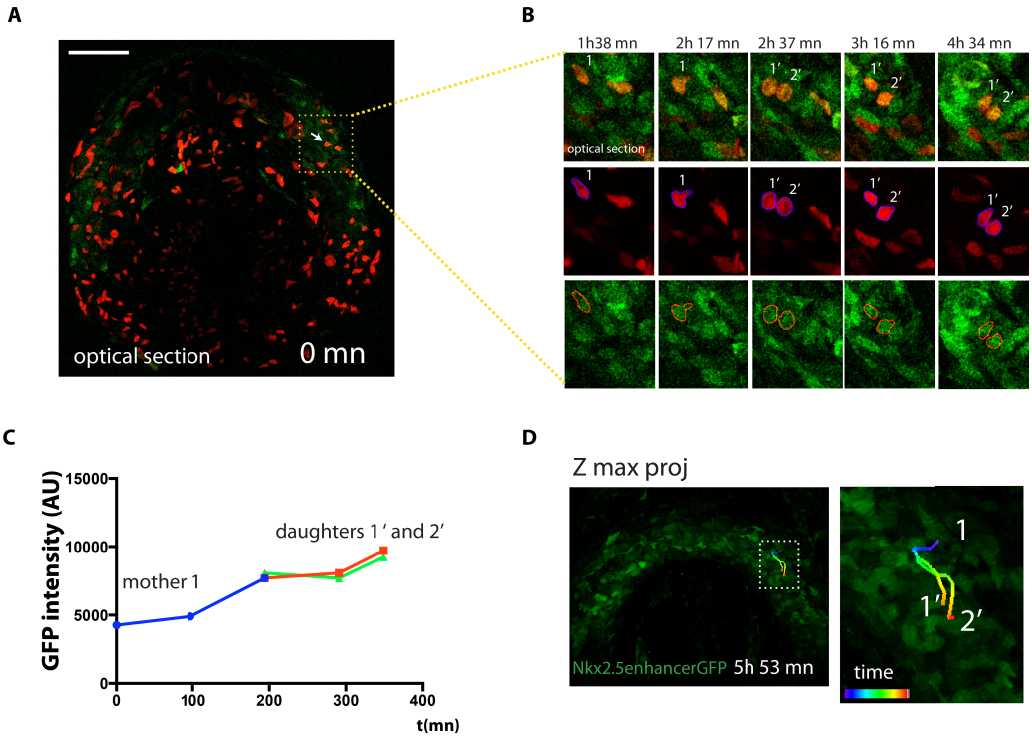

Figure 5–Figure supplement 1. Cells divide during cardiac differentiation. (A-C) Time-lapse movie of a dividing red-labelled tracked cell. Images are single optical sections (same dataset as shown in Figure 4A). The dividing red-labelled cell and daughter cells are segmented and mean GFP level is measured. (D) Full 4D track of the dividing cell showing close localization of the progeny in the cardiac crescent. Scale bars: 100 µm

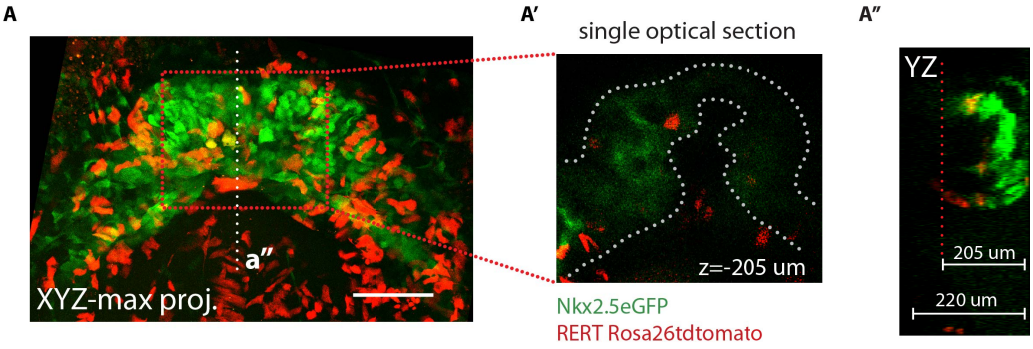

Figure 8–Figure supplement 1. GFP level in deeper z level cannot be accurately quantified.(A-A") R26tdtomato; Nkx2.5eGFP embryo at transversal HT stage. (A) z-maximum projection of 44 sections acquired every 5 µm and covering 220 µm. (A') single optical section at z=205 µm and showing weak GFP level corresponding to the red doter inset in (A). (A") yz view at the corresponding white dotted line shown in (A).